cmgh
CELLULAR AND MOLECULAR GASTROENTEROLOGY AND HEPATOLOGY

ORIGINAL RESEARCH

Prostaglandin E_2 and Akt Promote Stemness in Apc Mutant Dclk1 + Cells to Give Rise to Colitis-associated Cancer

Hayley J. Good,[1,2] Frederikke Larsen,[1,2] Alice E. Shin,[1,2] Liyue Zhang,[1,2] Mathieu Derouet,[1,2] David Meriwether,[3] Daniel Worthley,[4] Srinivasa T. Reddy,[3] Timothy C. Wang,[5] and Samuel Asfaha[1,2]

[1]Department of Medicine, University of Western Ontario, London, Ontario, Canada; [2]Verspeeten Family Cancer Centre, London Health Sciences Centre, London, Ontario, Canada; [3]Department of Medicine, Division of Cardiology, UCLA David Geffen School of Medicine, Los Angeles, California; [4]South Australian Health Medical Research Institute, North Terrace Adelaide, Australia; and [5]Division of Digestive and Liver Diseases, Department of Medicine, Columbia University, New York, New York

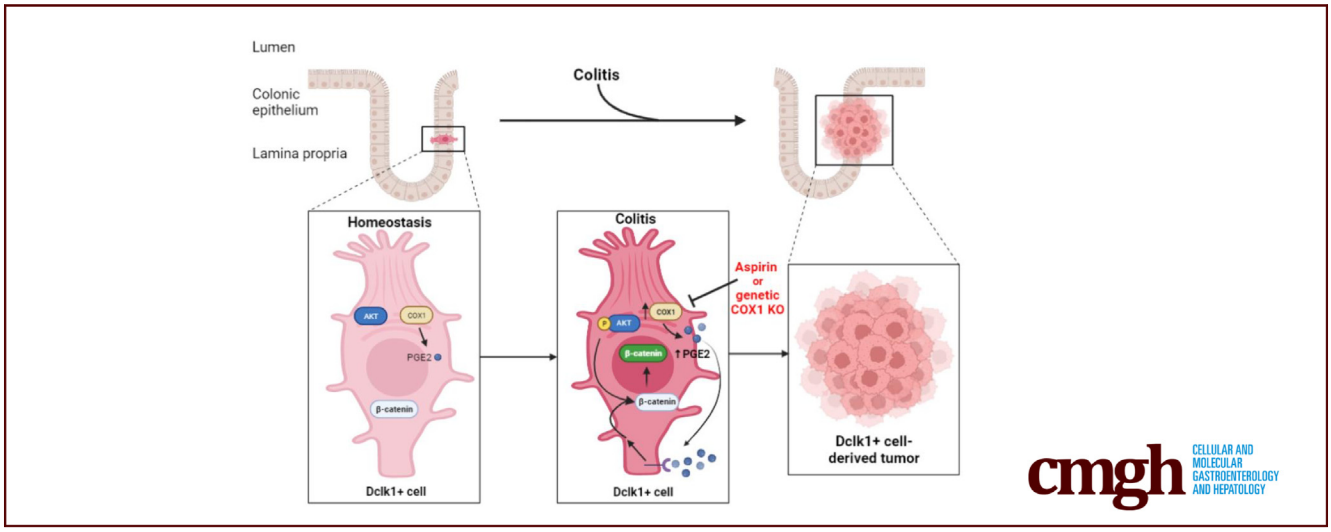

SUMMARY

We demonstrate that prostaglandin E_2 and Akt are increased in colitis prior to activation of Wnt signaling seen in inflammation-associated dysplasia. Inhibition of epithelial derived COX-1 either by aspirin or conditional knockout prevents development of colitis-associated cancer.

BACKGROUND & AIMS: Loss of the tumor suppressor gene Apc in Lgr5+ intestinal stem cells results in aberrant Wnt signaling and colonic tumorigenesis. In the setting of injury, however, we and others have also shown that non-stem cells can give rise to colonic tumors. The mechanism by which inflammation leads to cellular plasticity and cancer, however, remains largely unknown.

METHODS: RNA expression analysis of Wnt, COX, and Akt signaling was assessed in patients with quiescent or active ulcerative colitis (UC) and patients with UC-associated neoplasia using available datasets. The role of COX signaling in colonic tumorigenesis was examined using epithelial and doublecortin-like kinase 1 (Dclk1)+ cell-specific conditional COX-1 knockout mice and pharmacologic treatment with different nonsteroidal anti-inflammatory drugs.

RESULTS: In this study, we show that prostaglandins and phospho-Akt are key inflammatory mediators that promote stemness in Apc mutant Dclk1+ cells that give rise to colorectal cancer. Moreover, prostaglandin E_2 (PGE_2) and Akt are increased in colitis in both mice and humans, leading to inflammation-associated dysplasia upon activation of Wnt signaling. Importantly, inhibition of epithelial-derived COX-1 by aspirin or conditional knockout in Dclk1+ cells reduced PGE_2 levels and prevented the development of inflammation-associated colorectal cancer.

CONCLUSIONS: Our data shows that epithelial and Dclk1+ cell-derived COX-1 plays an important role in inflammation-associated tumorigenesis. Importantly, low-dose aspirin was effective in chemo-prevention through inhibition of COX-1 that reduced colitis-associated cancer. *(Cell Mol Gastroenterol Hepatol 2025;19:101469; https://doi.org/10.1016/j.jcmgh.2025.101469)*

Keywords: Aspirin; Colitis; Colon Cancer; Dclk1; Stem Cells.

This article has an accompanying editorial.

The intestine and colon are lined by a single layer of epithelial cells that turn over every few days. This rapid turnover of cells provides the gut lining with a remarkable ability to regenerate and heal upon injury. In homeostasis, rapidly dividing leucine-rich repeat-containing G protein-coupled receptor 5 (Lgr5) expressing stem cells at the crypt base maintain cell renewal, in large part, through Wnt signaling.[1] In the context of injury, however, cells higher in the crypt replenish epithelial cells, including Lgr5+ cells that are lost, and signaling occurs through the Hippo/YAP pathway,[2–6] with Sca1+ cells being described as key mediators of this epithelial repair.[3,5,7–11] Furthermore, Wnt plays a role in epithelial regeneration,[12–14] and this is believed to occur through canonical Wnt signaling in stem or progenitor cells.[15–17] When stem cell function is altered, the result is often impaired healing and/or uncontrolled epithelial cell proliferation.

Indeed, mutations leading to Wnt activation in specific intestinal epithelial cells result in tumorigenesis. In the case of sporadic colorectal cancer (CRC), Barker et al demonstrated that actively proliferating multipotent Lgr5+ stem cells rapidly give rise to colonic tumors upon loss of the *APC* gene, a tumor suppressor and negative regulator of the Wnt signaling pathway.[18] More recently, we and others have shown that non-stem cells (ie, post-mitotic cells) can also give rise to intestinal or colonic tumors, particularly in the setting of injury.[19–22] In the latter case, tumorigenesis is presumed to arise from the reversion of less differentiated cells to a facultative stem cell state. The mechanism by which inflammation leads to this cellular plasticity, however, is not known.

The association of chronic inflammation with cancer is well-described and supported by the clinical observation that patients with inflammatory bowel disease (IBD) are at an increased risk of colorectal cancer (CRC).[23–26] Thus, a better understanding of how inflammation disrupts the pathways regulating epithelial homeostasis will help elucidate how tumorigenesis arises following injury.

In this study, we demonstrate that prostaglandin and Akt signaling are upregulated in both patients and mice with inflammation-associated colonic dysplasia. Using a mouse model of colitis, we demonstrate that both prostaglandins and Akt directly lead to stemness (ie, dedifferentiation to a proliferating multipotent state) of doublecortin-like kinase 1 (Dclk1)+ cells and inflammation-associated tumors. Importantly, inhibition of prostaglandin synthesis by low-dose aspirin, but not COX-2 selective inhibitors, is effective in inhibiting stemness and preventing inflammation-associated cancer.

Results

Cyclooxygenase and Akt are Increased Prior to Wnt Activation During Inflammation-associated Colonic Tumorigenesis

Given that sporadic CRC is commonly associated with hyperactive Wnt signaling, we first confirmed that colitis-associated tumors in mice similarly show active Wnt activity. We examined canonical Wnt by localization of β-catenin in tumors from azoxymethane (AOM)/ dextran sodium sulfate (DSS)-treated mice or Dclk1^{CreERT2}; adenomatous polyposis coli (APC)$^{f/f}$ mice.[19] β-catenin immunofluorescence staining was restricted to the epithelial cell membrane in the normal colon, whereas β-catenin was detected in the cytoplasm and nucleus of colitis-associated tumors (Figure 1*A*), analogous to what was previously reported.[27–30] Active Wnt signaling in colitis-associated cancer (CAC) was further confirmed by the detection of elevated Wnt target genes in AOM/DSS-derived tumors compared with control tissues (Figure 1*B*).

To identify factors that could lead to Wnt activation and ultimately CAC, we compared the RNA expression of known Wnt mediators between control tissues and AOM/DSS-derived tumors. We found that Cox- and Akt-related gene expression was upregulated in mice with colitis-associated tumors vs non-neoplastic control tissues in AOM/DSS treated mice (Figure 1*C–D*). To better define the timeline of Wnt, Cox, and Akt- related gene expression, we next analyzed a publicly available dataset of gene expression from the AOM/DSS mouse model of CAC.[31] Cox and Akt gene expression was increased at early timepoints following colitis, whereas the majority of Wnt target genes were decreased (Figure 1*E*). Notably, Wnt target gene expression was increased compared with controls at later timepoints beyond 3 weeks after DSS colitis (Figure 1*E*).

To investigate if a similar pattern is observed in humans, we compared RNA expression of Wnt, Cox, and Akt-related genes in colonic tissue of patients previously reported to have quiescent ulcerative colitis and neoplasia (UCN) vs quiescent ulcerative colitis and no neoplasia (UC).[32] The colonic biopsies used for this study were taken from 5 healthy controls, 4 patients with quiescent UC, and 11 patients with quiescent UC that harbored a distant neoplastic lesion. We found that the prostaglandin synthase enzymes *COX-1*, *COX-2*, and *PTGES*, as well as the serine/threonine kinase *AKT3* were the most significantly upregulated genes in patients with UCN vs healthy controls. Patients with UC but no neoplasia, on the other hand, did not show increased COX and Akt signaling (Figure 1*F–G*). Notably, both prostaglandin E_2 (PGE_2) and phospho-Akt, mediators of COX and

Abbreviations used in this paper: **ANOVA, analysis of variance; AOM, azoxymethane; APC, adenomatous polyposis coli; CAC, colitis-associated cancer; CRC, colorectal cancer; Dclk1, doublecortin-like kinase 1; DSS, dextran sodium sulfate; EGFR, epidermal growth factor receptor; FBS, fetal bovine serum; FFPE, formalin-fixed paraffin-embedded; GPCR, G-protein coupled receptor; HTAB, hexadecyltrimethylammonium bromide; IBD, inflammatory bowel disease; IHC, immunohistochemistry; i.p., intraperitoneally; LC-MS, liquid chromatography-mass spectrometry; LOX, lipoxygenase; MPO, myeloperoxidase; MRM, multiple reaction monitoring; NSAIDS, nonsteroidal anti-inflammatory drugs; PBS, phosphate buffered saline; PG, prostaglandin; PGE2, prostaglandin E2; RT-PCR, reverse transcription polymerase chain reaction; UC, ulcerative colitis.**

Most current article

2352-345X
https://doi.org/10.1016/j.jcmgh.2025.101469

Akt signaling pathways, respectively, have previously both been shown to promote canonical Wnt signaling.[33–36] We did not, however, detect increased Wnt target gene expression in the colonic tissues of patients with quiescent UC, regardless of the presence or absence of neoplasia (Fig 1*F and H*). Taken together, these data suggest that increased Cox and Akt expression precedes the activation of Wnt seen in colitis-associated dysplasia or cancer.

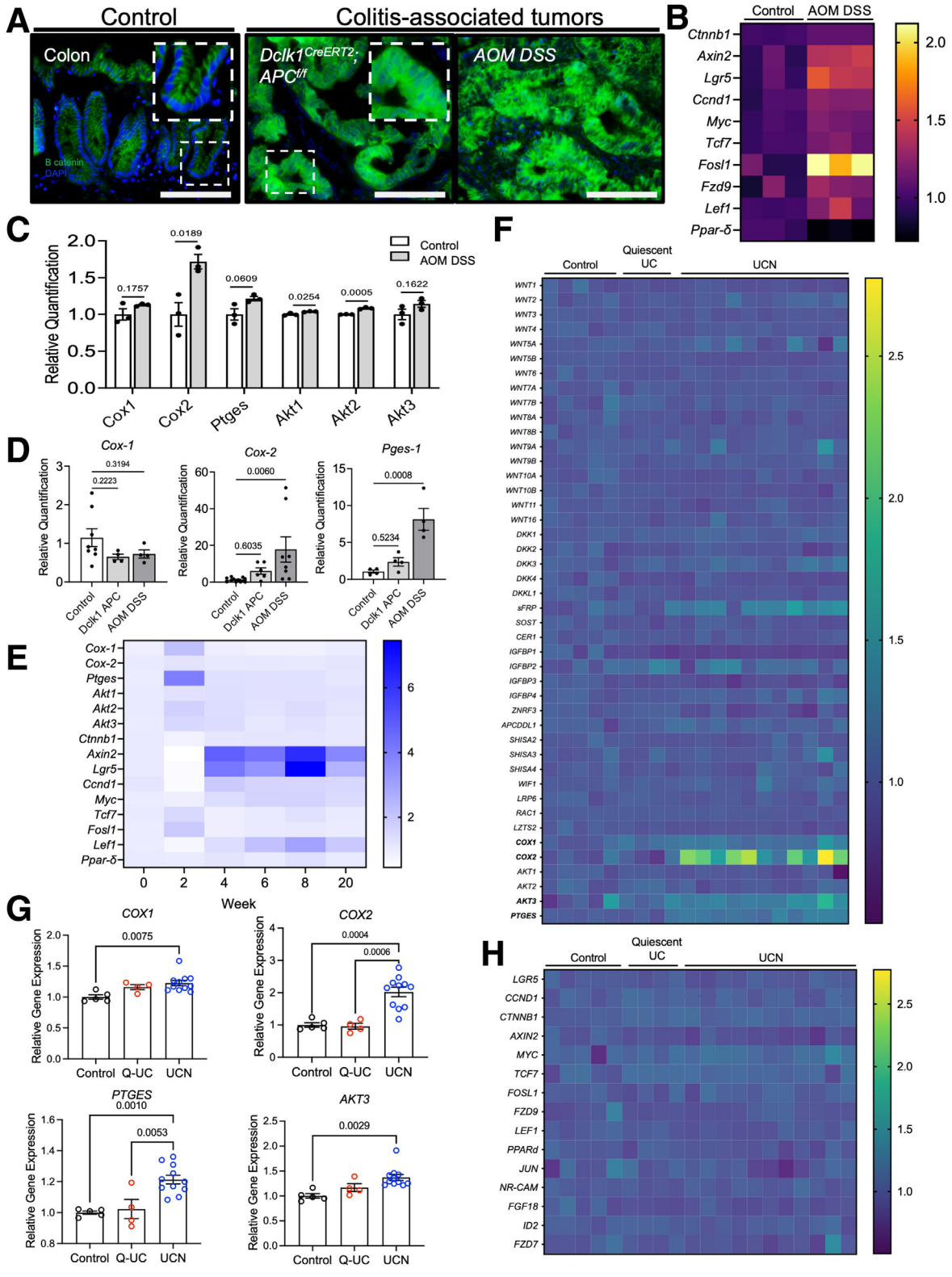

COX and Akt Signaling Pathways are Upregulated During Active Inflammation

Given that *COX* and *AKT* mRNA expression were increased prior to activation of Wnt signaling in patients with UC with quiescent disease and neoplasia, we next examined whether the expression of these mediators is altered during acute colitis. We first analyzed a publicly available gene expression dataset from patients with active vs quiescent UC.[36,37] In this analysis, RNA expression profiles of colonic samples from 11 controls, 23 patients with quiescent UC, and 74 patients with active UC were included (see Methods for additional patient details). We again found that *COX-1*, *COX-2*, *PTGES*, and *AKT3* expression were significantly increased in colonic tissues from patients with active UC vs healthy controls or patients with quiescent UC (Figure 2*A–B*). Wnt target genes, on the other hand, were unchanged or downregulated in active UC vs controls and quiescent UC, with the exception of Lef1, consistent with our observations in patients with dysplasia having increased Cox and Akt prior to Wnt activation (Figure 2*A*). To determine whether Cox and Akt are similarly upregulated in mouse models of colitis, we treated C57BL6/J wild-type mice with 2.5% DSS for 5 days and analyzed colonic tissues at the known time point of peak inflammation (day 8) and 2 weeks post-colitis (Figure 2*C*). We found the relative RNA transcript levels of *Cox-1* and *Cox-2* mRNA were increased in colonic tissues from DSS-treated mice vs controls (Figure 2*D*), and this persisted during the regenerative phase of colitis as late as 2 weeks post-colitis (Figure 2*E*).

Next, we assessed COX enzymatic activity in colitis by measuring the levels of COX-derived prostaglandins (PGs) in DSS colitis. Eicosanoids derived from both COX and lipoxygenase (LOX) enzymes, the 2 distinct pathways downstream of arachidonic acid metabolism, were measured by liquid chromatography-mass spectrometry (LC-MS) (Figure 2*F*). Our data revealed that all series-2 COX-, but not all LOX-derived lipid mediators were significantly increased in DSS-colitis, confirming that the COX pathway is active in colitis (Figure 2*G–H*). In particular, PGE_2 levels were upregulated in colonic tissues of DSS-treated mice compared with controls, and the PGE_2 metabolites, 15-keto PGE_2 and 13,14-dihydro-15k- PGE_2, were unchanged or downregulated, respectively (Figure 2*G*). These data suggest that during inflammation, PGE_2 is upregulated, whereas its metabolism is reduced, allowing for prolonged duration of activity. Furthermore, we observed increased activity of the Akt pathway in DSS-colitis as shown by increased phospho-Akt in DSS-treated mice (Figure 2*I–J*). Interestingly, aspirin decreased PGE_2 levels (Figure 2*L*) and prevented the increase in phospho-Akt levels during DSS-colitis (Figure 2*K*), suggesting that COX activity is important in the activation of Akt signaling during inflammation. Thus, our data suggest that both Cox activity and Akt signaling are upregulated in active colitis and that upregulation of Akt is, at least in part, linked to COX activity.

PGE_2 and Akt Activity Promote the Stemness of Mature Epithelial Dclk1+ Cells

Given that Cox and Akt were upregulated in active colitis and pre-neoplastic tissue of patients who developed CAC, we next examined the role of PGE_2 and Akt in the dedifferentiation of non-stem cells in the epithelium. To do this, we capitalized on our $Dclk1^{CreERT2}$;$R26^{mTmG}$;$APC^{f/f}$ ($APC^{f/f}$) transgenic mouse model of colitis-associated tumorigenesis. In this model, we previously showed that Dclk1-expressing epithelial cells serve as a cellular origin of colitis-associated tumors.[19] Therefore, in this study, we used these mice to examine the effects of misoprostol (PGE analogue) and SC79 (an Akt activator[38]) on Dclk1+ cell-derived lineage tracing. $Dclk1^{CreERT2}$;$R26^{mTmG}$ ($APC^{+/+}$) or $Dclk1^{CreERT2}$;$R26^{mTmG}$;$APC^{f/f}$ ($APC^{f/f}$) mice were given tamoxifen to specifically delete Apc in Dclk1-expressing cells, and subsequently treated with misoprostol and/or SC79 (Figure 3*A*). No lineage tracing was observed from Dclk1+ cells in either

Figure 1. (***See previous page***). **Active Wnt signaling in inflammation-associated tumors is preceded by increased COX and Akt expression.** (*A*) Representative immunofluorescent images of sections from control colonic tissue, $Dclk1^{CreERT}$/$APC^{f/f}$ colonic tumors, and AOM/DSS-derived colonic tumors. Scale bars = 100 μm. (*B*) Heatmap showing the relative mRNA expression of Wnt target genes in the colonic tissue of control mice (n = 3) and distal colonic tissue of mice with AOM/DSS-derived colonic tumors (n = 3). Data were derived from Gene Expression Omnibus (GEO) data set GSE44904 and normalized to control samples. (*C*) Relative mRNA expression of genes of Cox and Akt pathways in the colonic tissue of control mice (n = 3) and distal colonic tissue of mice with AOM DSS-derived colonic tumors (n = 3). Data were derived from GEO data set GSE44904 and normalized to control samples. Data are presented as mean ± SEM. Statistical significance was assessed by Student's unpaired *t*-test. (*D*) Relative mRNA expression of *Cox-1*, *Cox-2*, and *Pges-1* as analyzed by qPCR in colonic tumors derived from the $Dclk1^{CreERT2}$;$APC^{f/f}$ and AOM/DSS models of CAC relative to control colonic tissue. Data are presented as mean ± SEM and dots represent biologically independent animals (control, n = 8; $Dclk1^{CreERT2}$;$APC^{f/f}$, n = 4; AOM/DSS, n = 4). (*E*) Relative mRNA expression levels of Cox, Akt, and Wnt target genes in the colonic tissue of mice at weeks 2, 4, 6, 8, and 20 of disease progression in the AOM/DSS model of CAC (n = 3). Data were derived from GEO data set GSE31106 and normalized to baseline (time = 0) control samples. (*F*) Heatmap showing the relative mRNA expression of Wnt pathway modulators in the colonic tissue from healthy control subjects (n = 5), patients with quiescent UC (n = 4), or patients with UC-associated neoplasia (n = 11). Data were derived from GEO data set GSE37283 and normalized to control samples. (*G*) Relative mRNA expression of *COX-1*, *COX-2*, *PTGES*, and *AKT3* in the colonic tissue from healthy control subjects (n = 5), patients with quiescent UC (n = 4), or patients with UC-associated neoplasia (n = 11). Data were derived from GEO data set GSE37283 and normalized to control samples. Data are presented as mean ± SEM and dots represent biologically independent subjects. Statistical significance was assessed by ordinary one-way ANOVA with Tukey's post-hoc test. (*H*) Heatmap showing the relative mRNA expression of Wnt target genes in the colonic tissue from healthy control subjects (n = 5), patients with quiescent UC (n = 4), or patients with UC-associated neoplasia (UCN) (n = 11). Data were derived from GEO data set GSE37283 and normalized to control samples.

APC$^{+/+}$ or *APC*$^{f/f}$ vehicle-treated mice. Moreover, lineage tracing of crypts in APC$^{+/+}$ (wild-type) mice treated with misoprostol and/or SC79 was exceedingly rare (ie, only 1 traced crypt was detected in 14–20 sections analyzed per group in 25%–33% of mice). In contrast, SC79 and misoprostol treatment of *APC*$^{f/f}$ mice resulted in significantly increased Dclk1+ cell-derived lineage tracing (ie, 1 traced crypt was detected every 2–5 sections analyzed per group

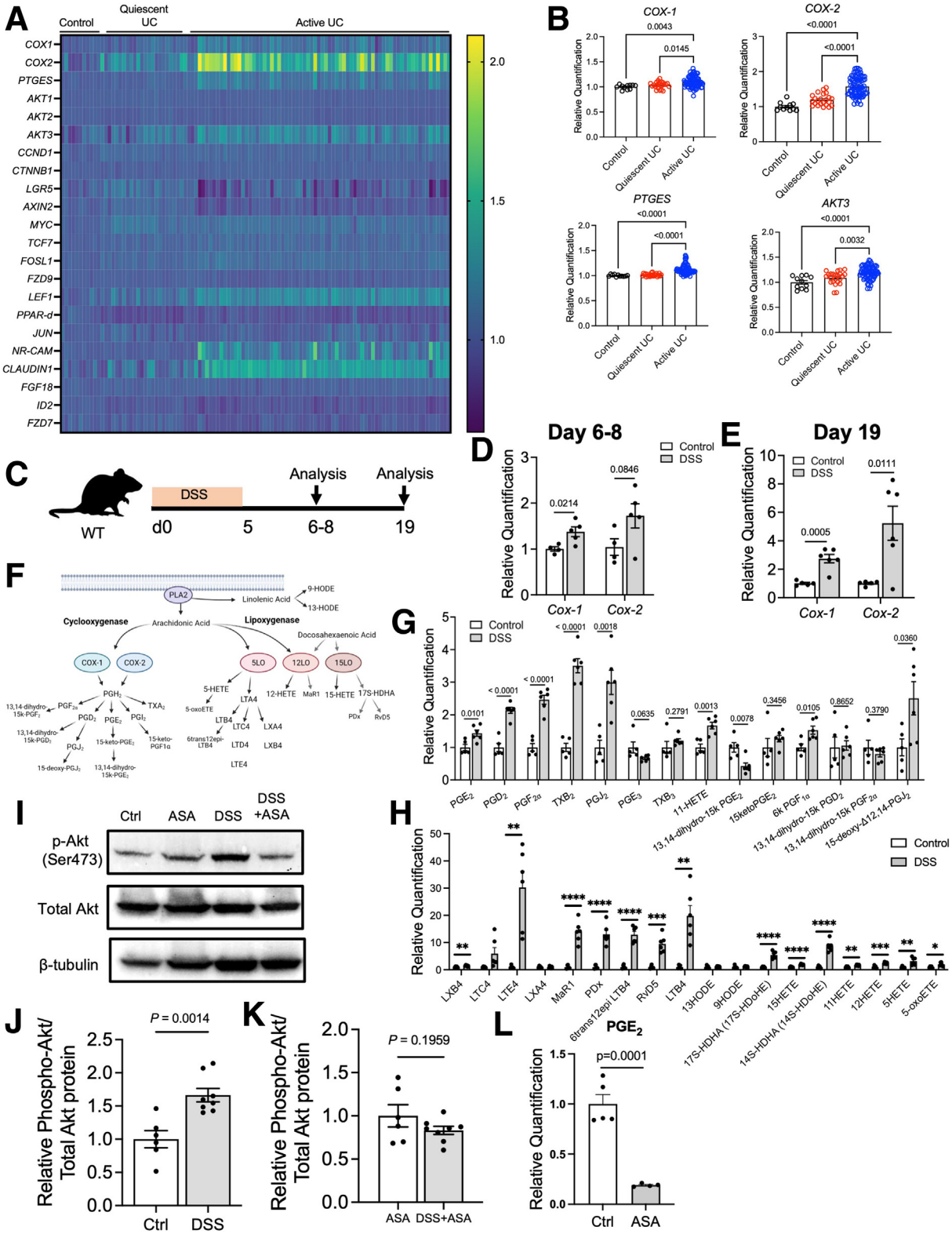

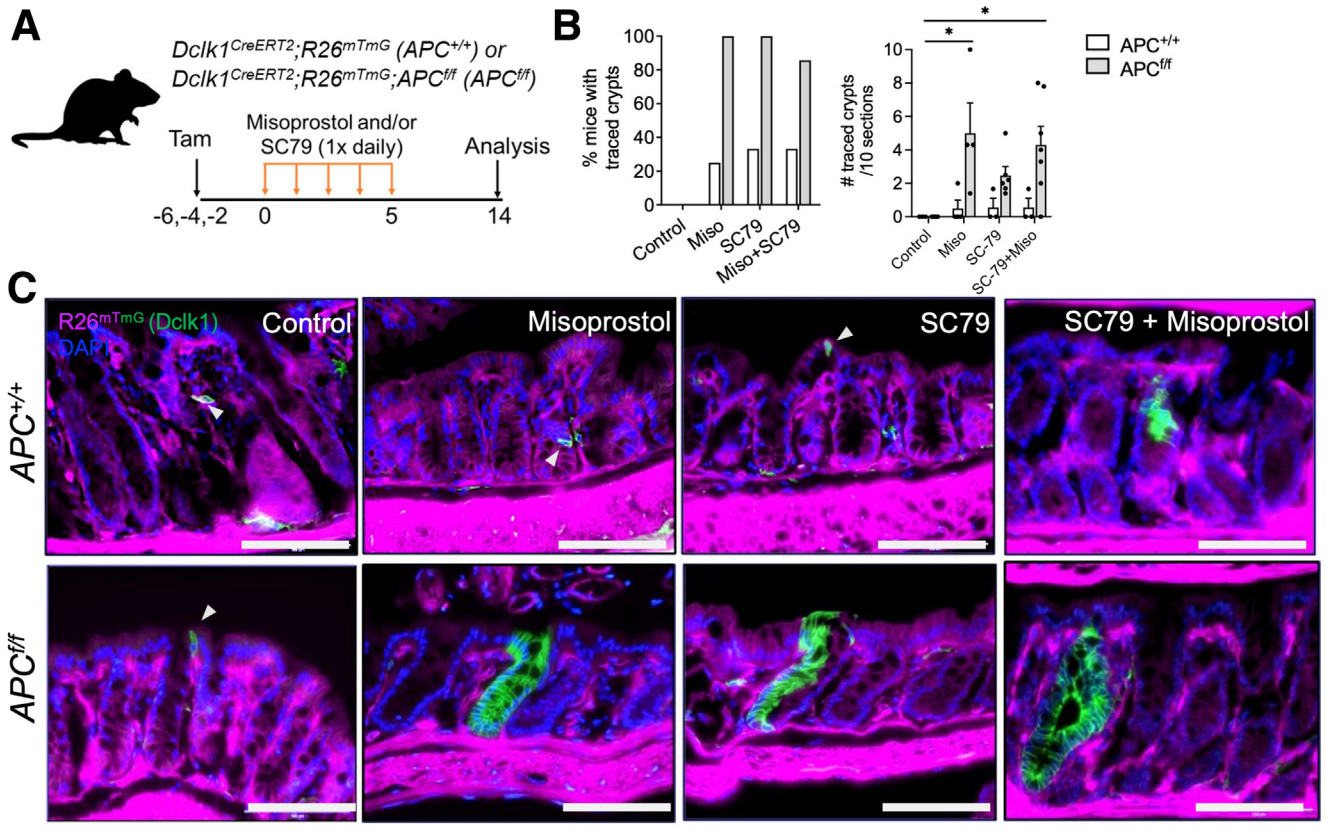

Figure 3. PGE_2 and Akt signaling promote epithelial Dclk1+ cell stemness *in vivo*. (*A*) Schematic illustration for the treatment of *Dclk1*^{CreERT2};*R26*^{mTmG} (*APC*$^{+/+}$) or *Dclk1*^{CreERT2};*R26*^{mTmG};*APC*$^{f/f}$ (*APC*$^{f/f}$) mice with Misoprostol (PGE analogue) and/or SC79 (Akt activator). (*B*) Quantification of the percentage of *APC*$^{+/+}$ or *APC*$^{f/f}$ mice (*left*) and the percentage of sections analyzed (*right*) with Dclk1+ cell-derived traced crypts upon treatment with SC79 and/or misoprostol. (*C*) Representative fluorescence microscopy images of the colonic epithelium with single Dclk1+ cells (white arrowheads) or Dclk1+ cell-derived lineage tracing (*APC*$^{+/+}$: control, n = 3; misoprostol, n = 4; SC79, n = 3; SC79 + misoprostol, n = 3; *APC*$^{f/f}$: control, n = 6; misoprostol, n = 4; SC79, n = 6; SC79 + misoprostol, n = 7). Scale bars = 100 μm.

Figure 2. (*See previous page*). Active colitis is associated with increased Akt and Cox signaling activity. (*A*) Heatmap showing the relative mRNA expression levels of Cox, Akt, and Wnt target genes in the colonic tissue from control subjects (n = 11), patients with active UC (n = 74), and patients with quiescent UC (n = 23). Data were derived from GEO data set GSE75214 and normalized to control samples. (*B*) Relative mRNA expression of *COX-1*, *COX-2*, *PTGES*, and *AKT3* in the colonic tissue from control subjects (n = 11), patients with active UC (n = 74), and patients with quiescent UC (n = 23). Data were derived from GEO data set GSE75214 and normalized to control samples. Data are presented as mean ± SEM and dots represent biologically independent subjects. Statistical significance was assessed by ordinary one-way ANOVA with Tukey's post-hoc test. (*C*) Schematic illustration of the DSS-colitis model. C57Bl/6 mice were administered 2.5% DSS in the drinking water for 5 days and analyzed on day 8 and 19. (*D*) Relative mRNA expression of *Cox-1* and *Cox-2* on day 8 in DSS-treated mice as analyzed by qPCR. Data are presented as mean ± SEM and dots represent biologically independent animals (control, n = 5; DSS, n = 6). (*E*) Relative mRNA expression of *Cox-1* and *Cox-2* on day 19 in DSS-treated mice as analyzed by qPCR. Data are presented as mean ± SEM and dots represent biologically independent animals (control, n = 4; DSS, n = 5). (*F*) Schematic of COX and LOX-derived inflammatory lipid metabolism. (*G*) Relative levels of COX-derived prostaglandins in DSS-treated mice as analyzed by LC-MS. Data are presented as mean ± SEM and dots represent biologically independent animals (control, n = 5; DSS, n = 6). (*H*) Relative levels of LOX-derived prostaglandins in DSS-treated mice as analyzed by LC-MS. Data are presented as mean ± SEM and dots represent biologically independent animals (control, n = 5; DSS, n = 6). (*I*) Western blot showing phospho-Akt and total Akt protein levels in DSS-colitis and upon COX inhibition with Aspirin (ASA). (*J*) Relative protein levels of phospho-Akt as compared to total Akt in DSS-colitis. Data are presented as mean ± SEM and dots represent biologically independent animals (control, n = 6; DSS, n = 8). (*K*) Relative protein levels of phospho-Akt as compared to total Akt during DSS-colitis upon COX inhibition by aspirin (ASA). Data are presented as mean ± SEM and dots represent biologically independent animals. (ASA, n = 6; DSS+ASA, n = 8). (*L*) Relative quantification of PGE_2 protein concentration between control (ctrl) and aspirin (ASA) treated mice. Data shown are mean ± SEM, and dots represent biologically independent animals (Ctrl, n = 5; ASA, n = 4).

and in 86%–100% of mice) (Figure 3*B*–*C*), suggesting that misoprostol and SC79 promote the stemness of Dclk1+ cells, particularly in the setting of Apc-loss.

To validate that Akt activation and PGE_2 induce stemness in Apc-deficient Dclk1+ cells, we additionally treated organoids from *Dclk1*^{CreERT2};*APC*$^{f/f}$;*R26*^{tdTomato} mice with PGE_2 and/or SC79 (Figure 4*A*). Indeed, treatment with PGE_2 and SC79 resulted in TdTomato+ lineage tracing from Apc-deficient Dclk1+ cells, an effect that was not observed in vehicle-treated organoids (Figure 4*B*–*C*). Next, we examined the effects of PGE_2 and Akt activation on the intestinal epithelium during injury. We induced epithelial injury

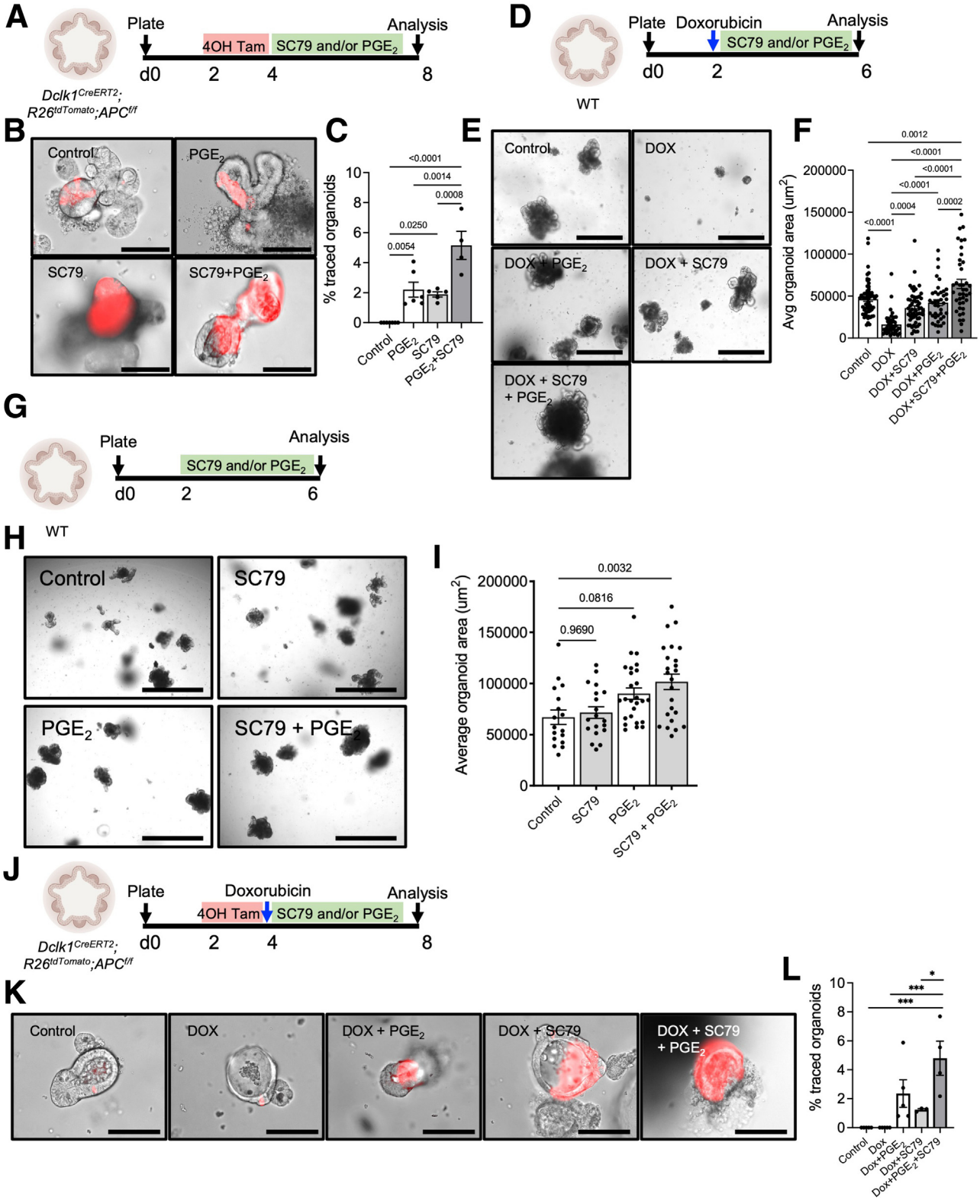

in vitro by treating organoids with the chemotherapeutic agent doxorubicin and then cultured the organoids in the presence of PGE_2 and/or SC79 (Figure 4*D*). Doxorubicin has previously been shown to induce DNA damage, leading to cell apoptosis and senescence.[39] Thus, we first confirmed that doxorubicin caused epithelial injury that reduced organoid size when compared with untreated controls (Figure 4*F*). Treatment with PGE_2 or SC79 after injury, however, abrogated the reduction in organoid size seen with doxorubicin injury. Interestingly, the combination of PGE_2 and SC79 resulted in even larger organoids than untreated control organoids or organoids treated with PGE_2 or SC79 alone (Figure 4*E–F*). These data suggest that PGE_2 and SC79 both promote organoid growth after injury, an effect that is further enhanced when present in combination. Notably, PGE_2 and SC79 also improved organoid growth of control uninjured organoids (Figure 4*G–I*). Thus, to next test whether this effect was mediated by promoting dedifferentiation of Dclk1+ cells, we next assessed the effects of Akt activation and PGE_2 on Dclk1+ cell expansion in injury. $Dclk1^{CreERT2};APC^{f/f};R26^{tdTomato}$ organoids were treated with doxorubicin (to induce injury) and subsequently cultured in the presence of SC79 and/or PGE_2 (Figure 4*J*). Incubation of doxorubicin-treated organoids in the presence of SC79 and PGE_2 led to Dclk1+ cell-derived lineage tracing, whereas vehicle-treated control organoids did not show any lineage tracing. These data confirm that SC79 and PGE_2 directly promote Dclk1+ cell stemness even in the setting of injury (Figure 4*K–L*). Taken together, these data suggest that PGE_2 and Akt signaling pathways promote stemness of Dclk1+ cells that have Apc-loss, particularly in the context of injury, where we observed dedifferentiation of Dclk1+ cells and lineage tracing of the crypts in vivo and lineage tracing of organoids in vitro.

PGE_2 and Akt Activation Promote Wnt Signaling and Lead to Inflammation-associated Dysplasia

To test whether Akt signaling and PGE_2 promote Dclk1+ cell stemness through activation of Wnt signaling, we next analyzed the cellular localization of β-catenin in colonic crypts lineage traced by *Apc*-deficient Dclk1+ cells treated with misoprostol and/or SC79 treatment. Consistent with our previous observation, we found that *Apc*-deficient Dclk1+ cells display membrane-bound β-catenin, indicative of inactive Wnt signaling[19] (Figure 5*A*). In mice treated with misoprostol or SC79 alone, β-catenin remained localized to the membrane in Dclk1+ cell lineage-traced crypts. In contrast, the combination of misoprostol plus SC79 resulted in Dclk1+ cell-derived lineage tracing associated with β-catenin localized to the nucleus (observed in ∼60% of crypts analyzed) (Figure 5*B–C*). Consistent with this observation, SC79 plus misoprostol treatment resulted in significantly increased mRNA expression of several Wnt target genes in colonic tissue (*Lgr5*, *C-myc*, *Ccnd1*, and *Ppar-delta*) compared with control (Figure 5*D*). These data suggest that the co-activation of PGE_2 and Akt signaling is able to promote active Wnt signaling in *Apc*-deficient Dclk1 + cells.

To next examine whether PGE_2 and Akt activation of Wnt signaling can promote tumorigenesis, we treated $Dclk1^{CreERT2};APC^{f/f};R26^{mTmG}$ mice with misoprostol and/or SC79 during DSS colitis (Figure 5*E*). We first titrated the dose of DSS to a level that allowed us to induce Dclk1+ cell-derived lineage tracing without inducing dysplasia (ie, only 15% of traced crypts showed dysplasia using 0.5% DSS) (Figure 5*F–G*). Administration of either SC79 or misoprostol concurrently with 0.5% DSS had no effect on the frequency of lineage tracing or dysplasia detected when compared with DSS alone (Figure 5*F and I–J*). However, concurrent administration of both misoprostol and SC79 led to increased Dclk1+ cell-derived dysplasia when compared with the vehicle-treated controls (ie, dysplasia was observed in 80% of traced crypts with misoprostol plus SC79 treatment vs 15% of traced crypts with vehicle treatment) (Figure 5*F–H*). Interestingly, the proportion of sections with traced crypts was not different when compared with vehicle (Figure 5*I–J*). The presence of dysplastic glands and the ability of PGE_2 and Akt activation to induce Wnt signaling was further confirmed by the localization of β-catenin in the

Figure 4. (***See previous page***). **PGE_2 and Akt signaling promote stemness of Dclk1+ cells in organoids.** (*A*) Schematic illustration for the treatment of $Dclk1^{CreERT2};R26^{tdTomato};APC^{f/f}$ organoids with SC79 and/or PGE_2. (*B*) Representative brightfield and fluorescent images of $Dclk1^{CreERT2};R26^{tdTomato};APC^{f/f}$ organoids treated with SC79 and/or PGE_2. Scale bars = 100 μm. (*C*) Quantification of the percentage of $Dclk1^{CreERT2};R26^{tdTomato};APC^{f/f}$ organoids showing Dclk1+ cell-derived lineage tracing upon treatment with SC79 and/or PGE_2. Data are presented as mean ± SEM, and dots represent biologically independent animals (control, n = 7; PGE_2, n = 6; SC79, n = 5; PGE_2 + SC79, n = 4). (*D*) Schematic illustration for the treatment of WT organoids treated with doxorubicin (DOX) plus SC79 and/or PGE2. (*E*) Representative brightfield images of WT organoids treated with doxorubicin plus SC79 and/or PGE_2. Scale bars = 200 μm. (*F*) Quantification of the average organoid area of WT organoids treated with doxorubicin plus SC79 and/or PGE_2. Data are presented as mean ± SEM, and dots represent individual organoids from n = 3 biologically independent animals. (*G*) Schematic illustration for the treatment of WT organoids treated with SC79 and/or PGE_2. (*H*) Representative brightfield images of WT organoids treated with SC79 and/or PGE_2. Scale bars = 100 μm. (*I*) Quantification of the average organoid area of WT organoids treated with SC79 and/or PGE_2. Data are presented as mean ± SEM, and dots represent individual organoids from n = 3 biologically independent animals. (*J*) Schematic illustration for the treatment of $Dclk1^{CreERT2};R26^{tdTomato};APC^{f/f}$ organoids with doxorubicin plus SC79 and/or PGE_2. (*K*) Representative brightfield and fluorescent images of $Dclk1^{CreERT2};R26^{tdTomato};APC^{f/f}$ organoids treated with doxorubicin plus SC79 and/or PGE_2. Scale bars = 100 μm. (*L*) Quantification of the percentage of $Dclk1^{CreERT2};R26^{tdTomato};APC^{f/f}$ organoids showing Dclk1+ cell-derived lineage tracing upon treatment with doxorubicin plus SC79 and/or PGE_2. Data are presented as mean ± SEM, and dots represent biologically independent animals (control, n = 5; DOX, n = 5; DOX + SC79, n = 5; DOX + PGE_2, n = 3; DOX + PGE_2 + SC79, n = 4).

nucleus within Dclk1+ cell GFP-lineage traced crypts derived from SC79 and misoprostol treatment (Figure 5*K*). Taken together, these data suggest that the co-activation of Akt and PGE2 promotes Wnt in Apc mutant Dclk1+ cells that stimulates these cells to give rise to dysplastic lesions during injury.

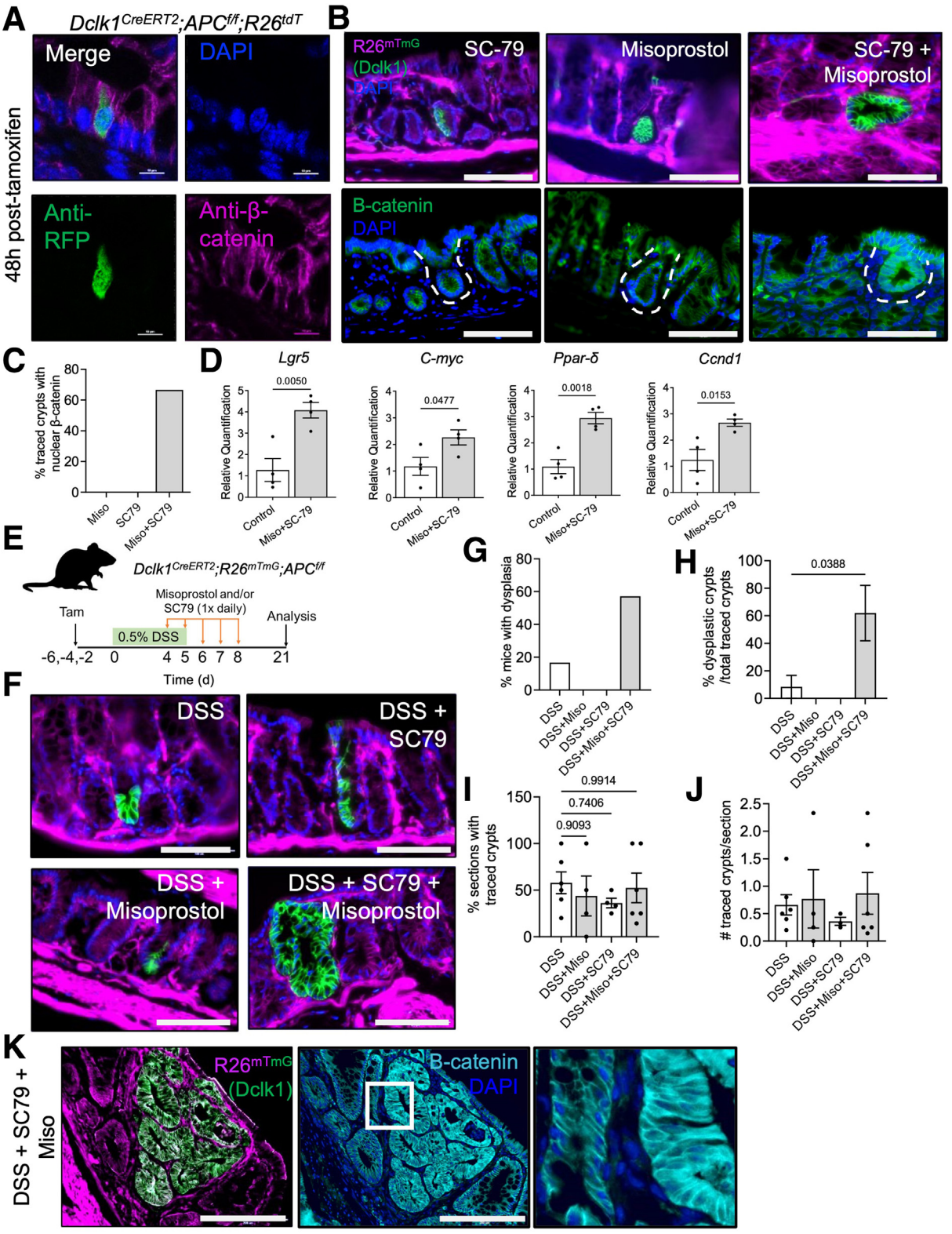

Inhibition of COX-1 Prevents Inflammation-associated Cancer

To next examine whether inhibition of PGE_2 synthesis can inhibit inflammation-associated cancer, we utilized nonsteroidal anti-inflammatory drugs (NSAIDs) that selectively inhibit COX-1 and/or COX-2 activity, in 2 models of CAC. First, we treated $Dclk1^{CreERT2}$;$APC^{f/f}$ mice with 2.5% DSS in the drinking water for 5 days to induce colonic inflammation, and then administered various NSAIDs 3 times during DSS and every day thereafter until the experimental endpoint at 14 weeks post-DSS (Figure 6*A*). We compared aspirin (a non-selective COX inhibitor) to the COX-2-selective inhibitors celecoxib and rofecoxib, the COX-1-selective inhibitor SC-560, and the non-selective COX-inhibitor indomethacin. Due to the reported potential toxicity of NSAIDs in patients with IBD and mice with colitis, we used doses corresponding to human-equivalent low-dose aspirin.

Treatment with aspirin significantly reduced tumor number but had no effect on tumor size (Figure 6*B–C*). In contrast, the COX-2 inhibitors had no effect on tumor number, whereas SC-560 and indomethacin both reduced tumor number, although this effect was only statistically significant in indomethacin-treated animals (Figure 6*B*). Neither COX-2 inhibitor, SC-560, nor indomethacin affected tumor size (Figure 6*C*). These data show that inhibition of COX activity can prevent inflammation-associated tumorigenesis and that COX-1 inhibition may be more important for chemoprevention.

We further validated our observations by testing COX-1 and -2 inhibitors in a second model of CAC. Wild-type C57Bl/6 mice were administered the carcinogen AOM (10 mg/kg intraperitoneally [i.p.]), followed by 2.5% DSS in the drinking water. NSAIDs were then administered 3 times during DSS and every day thereafter until the experimental endpoint at 20 weeks post-AOM (Figure 6*E*). Analogous to the $Dclk1^{CreERT2}$;$APC^{f/f}$ model, aspirin, SC-560, and indomethacin, but not celecoxib or rofecoxib, reduced colonic tumor number in the AOM/DSS model (Figure 6*F*). Similarly, there was no difference in tumor size, survival, or body weight observed among any of the treatment groups (Figure 6*G–H*). These data suggest that inhibition of COX-1, as opposed to COX-2, is most likely responsible for inhibition of colitis-induced tumorigenesis.

Importantly, when we tested if higher (anti-inflammatory) doses of COX-2 inhibitors could affect tumorigenesis, we observed 50% of mice experienced acute mortality (Figure 6*I*). These data suggest that in acute colitis, high-dose COX-2 inhibitors are not a feasible option for chemoprevention. In contrast, mice treated with low-dose aspirin not only had 100% survival but also had no change in body weight when compared with the vehicle or other NSAID-treated groups in both tumor models (Figure 6*D and H*). These findings suggest that low-dose aspirin does not exhibit the toxicity as that seen with COX-2 inhibitors in colitis.

We next confirmed that reduced tumor initiation upon COX-1 inhibition was due to the downregulation of PGs during inflammation. We performed LC-MS measurement of PG levels in mice with DSS-colitis treated with various NSAIDs vs vehicle (expression shown as relative to DSS-treated mice). Treatment with both aspirin (non-selective COX inhibitor) and SC-560 (a COX-1 inhibitor) during DSS colitis strongly reduced PG levels relative to DSS alone, whereas celecoxib (a COX-2 inhibitor) had much weaker efficacy (Figure 6*J–K*). We found that the proportion of PGs downregulated by the NSAIDs was largely due to inhibition of COX-1 (Figure 6*L*), suggesting that this COX isoform is the predominant source of colonic PGs in inflammation. Given that both aspirin and SC-560 inhibited colonic tumor formation, whereas celecoxib did not, we further identified the PGs that were differentially downregulated among NSAIDs during colitis. We found that 9 PGs were differentially downregulated by aspirin and SC-560 compared with

Figure 5. (***See previous page***). **PGE_2 and Akt activation promote Wnt signaling and lead to dysplasia.** (*A*) $Dclk1^{CreERT2}$;$R26^{tdTomato}$;$APC^{f/f}$ mice were treated with tamoxifen and analyzed at 48 hours. Representative immunofluorescent images for Dclk1+ cells (anti-RFP) and associated β-catenin immunostaining. Scale bars = 10 μm. (*B*) Representative immunofluorescent images of β-catenin immunostaining of Dclk1+ cell-derived traced colonic crypts induced by treatment of SC79 and/or Misoprostol. Scale bars = 100 μm. (*C*) Quantification of the percentage of Dclk1+ cell-derived traced colonic crypts with nuclear β-catenin localization. (*D*) Relative mRNA expression of Wnt target genes in colonic tissue of mice treated with misoprostol and SC79 as analyzed by qPCR. Data are presented as mean ± SEM, and dots represent biologically independent animals (control, n = 4; miso + SC79, n = 4). (*E*) Schematic illustration for the treatment of $Dclk1^{CreERT2}$;$R26^{mTmG}$;$APC^{f/f}$ mice with 0.5% DSS plus SC79 and/or PGE_2. (*F*) Representative fluorescence microscopy images of the colonic epithelium with Dclk1+ cell-derived lineage traced crypts upon treatment with DSS plus SC79 or Misoprostol, or Dclk1+ cell-derived lineage traced dysplastic lesions upon treatment with DSS plus SC79 and misoprostol. Scale bars = 100 μm. (*G*) Quantification of percentage of mice with Dclk1+ cell-derived dysplastic lesions upon treatment with DSS plus SC79 and/or misoprostol. (DSS, n = 6; DSS + Miso, n = 4; DSS + SC79, n = 4; DSS + Miso + SC79, n = 6). (*H*) Quantification of the percentage of Dclk1+ cell-derived lineage traced dysplastic lesions over the total number of tracing events upon treatment with DSS plus Misoprostol and/or SC79. (*I*) Quantification of the percentage of sections with Dclk1+ cell-derived traced crypts upon treatment with DSS plus Misoprostol and/or SC79. Data are presented as mean ± SEM, and dots represent biologically independent animals (DSS, n = 6; DSS + Miso, n = 4; DSS + SC79, n = 4; DSS + Miso + SC79, n = 6). (*J*) Quantification of the number of Dclk1+ cell-derived lineage traced crypts per section analyzed upon treatment with DSS plus SC79 and/or Misoprostol. Data are presented as mean ± SEM, and dots represent biologically independent animals (DSS, n = 6; DSS + Miso, n = 4; DSS + SC79, n = 4; DSS + Miso + SC79, n = 6). (*K*) Representative immunofluorescent images of β-catenin immunostaining of Dclk1+ cell-derived traced dysplastic lesions upon treatment with DSS plus SC79 and misoprostol. Scale bars = 200 μm.

celecoxib, including PGE_2 (Figure 6*M*). Taken together, these data demonstrate that COX-1 inhibition is effective in preventing inflammation-associated tumorigenesis via downregulation of prostaglandins, particularly PGE_2.

To further assess the safety of low-dose NSAIDs during colitis, we examined whether low-dose aspirin alters the severity of DSS colitis during the peak of inflammation (Figure 7*A*). Three days post-DSS, aspirin-treated mice had

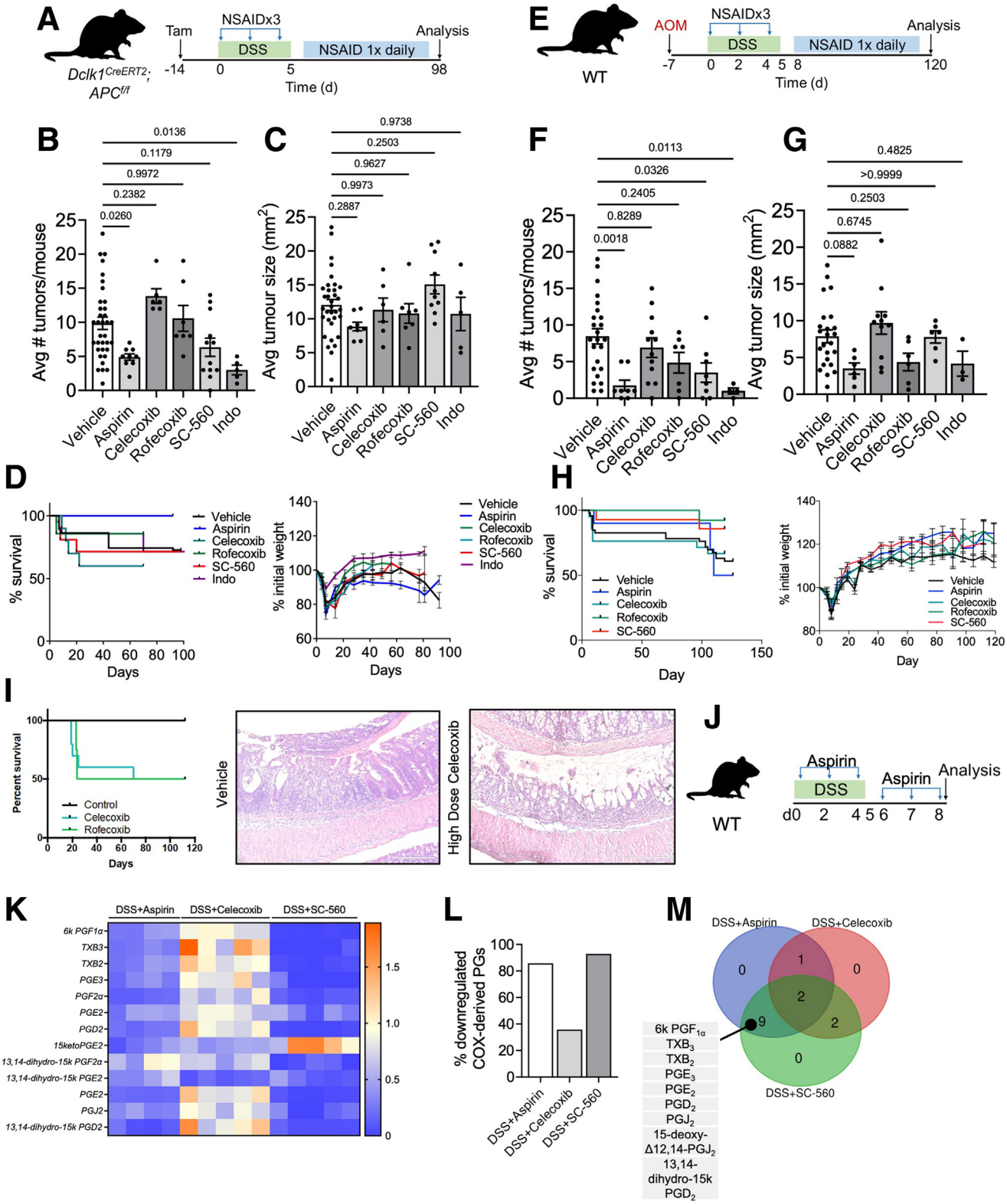

no significant change in histologic damage, cell proliferation, myeloperoxidase (MPO) activity, or levels of colonic inflammatory cytokines compared with vehicle-treated controls (Figure 7*B–H*). Similarly, aspirin had no significant effect on histologic damage or MPO activity during the regenerative phase of DSS colitis at day 19 but did reduce body weight loss during peak inflammation compared with mice treated with DSS alone (Figure 7*I–M*). These findings suggest that low-dose aspirin is safe to use during colitis in mice for the prevention of inflammation-associated tumorigenesis.

Loss of COX-1 Inhibits Inflammation-associated Cancer

To confirm that specifically COX-1 inhibition prevents the initiation of CAC, we generated *Krt19*$^{(BAC)\text{-}Cre}$;*COX-1*$^{f/f}$ mice that have constitutive loss of COX-1 in all intestinal epithelial cells. *Krt19*$^{(BAC)\text{-}Cre}$;*COX-1*$^{f/f}$ mice treated with AOM/DSS had significantly reduced colonic tumors compared with their Cre-negative littermates, but no change in tumor size (Figure 8*A–C*). These findings suggest that COX-1 inhibition, specifically in intestinal epithelial cells, prevents the initiation of CAC in mice.

To further examine if Dclk1+ cell-derived COX-1 expression is important in colitis-associated tumorigenesis, we crossed our *Dclk1*^{CreERT2};*APC*$^{f/f}$ model to *COX-1*$^{f/f}$ mice to conditionally knockout COX-1 specifically in Dclk1+ cells. To assess the effects of COX-1 loss on tumor initiation, we analyzed these mice acutely at day 21 after tamoxifen and 1.5% DSS treatment (Figure 8*D*). *COX-1*$^{f/f}$ mice had significantly fewer Dclk1+ lineage traced dysplastic lesions when compared with *COX-1*$^{+/+}$ mice (Figure 8*E–F*). These data indicate that COX-1 derived from Dclk1+ cells is important for the initiation of CAC. Indeed, mice with loss of COX-1 in Dclk1+ cells had fewer tumors than mice with intact COX-1 expression (Figure 8*G–H*). These data suggest that COX-1 in Dclk1+ cells plays an important role in inflammation-associated tumorigenesis (Figure 8*I*).

Discussion

Following intestinal injury, Lgr5+ stem cells are lost, and epithelial restitution originates from Lgr5-negative stem or progenitor cells.[2–6] During this epithelial repair, abnormal Wnt signaling in non-stem cells can lead to cellular plasticity and tumor development.[19,20] In this study, we show that COX and Akt signaling are upregulated during colitis and in dysplasia prior to the activation of Wnt in colitis-associated tumors. These findings suggest that the preceding upregulation of COX and Akt signaling may contribute to Wnt activation seen later in colorectal tumors.[27,29] Indeed, we demonstrate that activation of PGE_2 and Akt signaling in colitis leads to cellular plasticity of normally quiescent Dclk1+ cells to a stem cell state that allows for cancer initiation.

In the context of injury, non-stem cells have previously been shown to acquire stem cell properties that allow them to regenerate the epithelium.[3,5,40–46] Interestingly, PGE_2 not only contributes to intestinal regeneration through Yap[47] and/or Akt signaling,[35] but it also has been linked to stemness in a variety of tissues outside of the gastrointestinal tract.[48–53] For instance, in zebrafish, PGE_2 is necessary for Wnt activation in hematopoietic stem cells,[34] and in mice, it can promote the expansion of Lgr5+ stem cells in the intestine.[54] Consistent with these observations, our study further demonstrates that PGE_2 can contribute to the transformation of quiescent APC-mutant Dclk1+ cells to a multipotent colonic stem cell that drives inflammation-associated cancer initiation.

Notably, PGE_2 and Akt promoted stem cell capacity in Dclk1+ cells that were Apc-deficient. This observation suggests that PGE_2 and Akt act in concert to induce Wnt signaling and promote stemness in a previously "primed" Dclk1+ cell. More importantly, the simultaneous activation of PGE_2 and Akt signaling led Dclk1+ cells to give rise to dysplasia upon additional injury. These findings suggest that upregulation of PGE_2 and Akt activation seen during colitis may lead to the "second-hit" required to activate Wnt

Figure 6. (***See previous page***). **Downregulation of PGE_2 by inhibition of COX-1 and not COX-2 prevents inflammation-associated cancer.** (*A*) Schematic illustration for the treatment of *Dclk1*^{CreERT2};*APC*$^{f/f}$ mice with DSS and COX-inhibition by daily oral gavage of low-dose NSAIDs (aspirin, 25 mg/kg; celecoxib, 6 mg/kg; rofecoxib, 5 mg/kg; SC-560, 10 mg/kg; indomethacin, 1 mg/kg). (*B–C*) Average colonic tumor number (*left*) and size (*right*) of *Dclk1*^{CreERT2};*APC*$^{f/f}$ mice treated with vehicle or NSAIDs. Data are presented as mean ± SEM, and dots represent biologically independent animals (control, n = 41; aspirin, n = 9; celecoxib, n = 6; rofecoxib, n = 7; SC-560, n = 10; indomethacin, n = 5). (*D*) Survival curve (*left*) and body weight (*right*) for *Dclk1*^{CreERT2};*APC*$^{f/f}$ mice treated with NSAIDs during DSS and tumorigenesis. (*E*) Schematic illustration for the treatment of C57Bl/6 mice with AOM/DSS and COX-inhibition by daily oral gavage of low-dose NSAIDs (aspirin, 25 mg/kg; celecoxib, 6 mg/kg; rofecoxib, 5 mg/kg; SC-560, 10 mg/kg; indomethacin, 1 mg/kg). (*F–G*) Average colonic tumor number (*left*) and size (*right*) of C57Bl/6 mice treated with AOM/DSS and vehicle or NSAIDs. Data are presented as mean ± SEM, and dots represent biologically independent animals (control, n = 34; aspirin, n = 8; celecoxib, n = 6; rofecoxib, n = 7; SC-560, n = 8; indomethacin, n = 4). (*H*) Survival curve (*left*) and body weight (*right*) mice treated with NSAIDs during the AOM/DSS model of tumorigenesis. (*I*) Survival curve for *Dclk1*^{CreERT2};*APC*$^{f/f}$ mice treated with high-dose COX-2 inhibitors during and after DSS-colitis (*left*) and corresponding representative histological images of colonic tissue of mice treated with DSS or high-dose celecoxib plus DSS (*right*). (*J*) Schematic illustration for the treatment of C57Bl/6 mice with 2.5% DSS and COX-inhibition by NSAIDs. (*K*) Heatmap showing the relative levels of COX-derived prostaglandins in DSS-colitis upon treatment with aspirin (non selective COX inhibitor, n = 4), celecoxib (COX-2 inhibitor, n = 5), or SC-569 (COX-1 inhibitor, n = 5). (*L*) Quantification of the percentage of prostaglandins significantly downregulated or unchanged upon treatment with each NSAID. (*M*) Identification of prostaglandins downregulated upon treatment with aspirin and SC-560, but not celecoxib, during DSS relative to DSS alone.

signaling and initiate proliferation that ultimately gives rise to tumors from a mutated Dclk1+ cell.

PGE_2 has previously been shown to trans-activate the epidermal growth factor receptor (EGFR) and stimulate downstream activation of Akt in cancer.[55] Moreover, the combined use of COX and EGFR kinase inhibitors has been shown to be more potent for the prevention of colonic neoplasia than either drug alone, suggesting that PGE_2 and

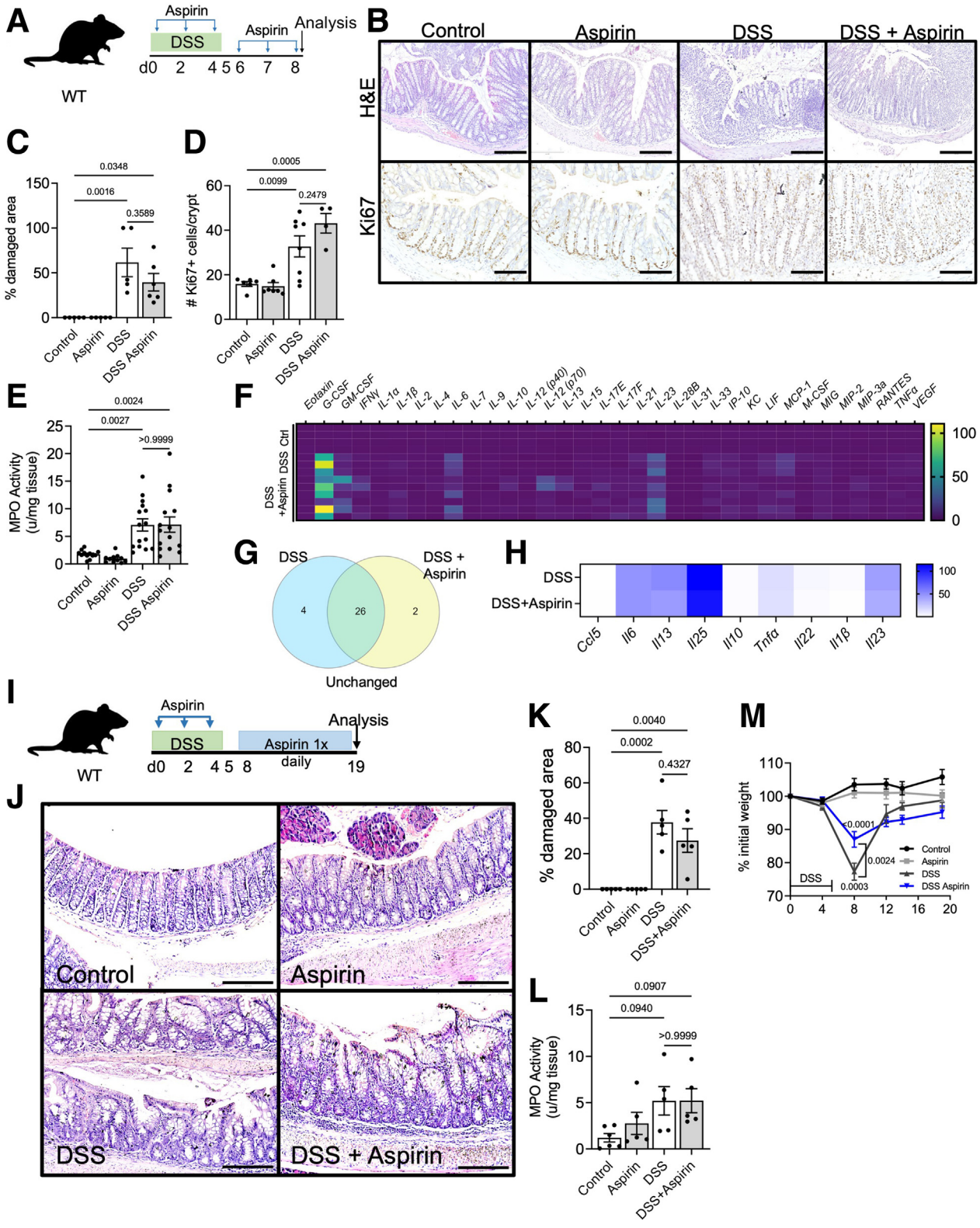

Akt may act in a synergistic manner to promote tumorigenesis.[56] Our findings similarly show that simultaneous activation of Akt and PGE_2 signaling is required for tumorigenesis, consistent with the notion that the effects of Akt activation are independent of PGE_2. Furthermore, the ability of PGE_2 to promote stemness has been linked to its ability to stimulate nuclear accumulation of β-catenin.[33,36,50] Phosphorylation of Akt stimulates the nuclear localization of β-catenin through both PGE_2-dependent and independent mechanisms. Our findings suggests that the combination of PGE_2 and Akt activation drives nuclear localization of β-catenin in *Apc*-deficient Dclk1+ cells to promote stemness and tumorigenesis. These findings are also consistent with the observations of Hayakawa et al, who reported that G-protein coupled receptor (GPCR) signaling is required for stimulation of nuclear β-catenin in *Apc*-deficient cells and that PGE_2 binds to 1 of the 4 GPCRs, EP1-4.[57]

The cellular and enzymatic source of PGE_2 that is most important in colitis-associated tumorigenesis is not known. In sporadic CRC, numerous studies have reported COX-2 to be the most important COX isoform.[49,58–61] However, our data suggests that inhibition of COX-1, rather than COX-2, is most important for prevention of colitis-associated tumorigenesis. Indeed, low-dose COX-2 inhibitors were not effective in preventing the initiation of CAC, whereas higher (anti-inflammatory equivalent) doses of COX-2 inhibitors were associated with increased mortality in the setting of colitis. This is consistent with previous reports that COX-2 inhibitors exacerbate colitis,[62–66] and that COX-1 also plays an important role in inflammation,[67–69] tumor initiation, early polyp growth,[58,70] and epithelial stem cell proliferation.[71] In this study, using our $Krt19^{(BAC)\text{-}Cre}$ and $Dclk1^{CreERT2}$;$APC^{f/f}$ models, we demonstrate that epithelial-derived and more specifically, Dclk1+ cell-derived COX-1, is an important driver of colitis-associated colonic tumorigenesis.

Taken together, our study provides novel insight into the mechanism by which inflammation leads to the transformation of non-stem cells during tumorigenesis. We demonstrate that COX-1-derived PGE_2 and p-Akt signaling are both upregulated in colitis and cooperate to promote stemness in Apc-deficient Dclk1+ cells during cancer initiation. This cellular plasticity is, at least in part, mediated through Wnt signaling and the promotion of nuclear translocation of β-catenin. Importantly, we demonstrate that low-dose aspirin prevents colitis-associated cancer by blocking production of COX-1-derived PGE_2, demonstrating its safety and effectiveness as a chemo-preventative drug in colitis.

Materials and Methods

Mice

Dclk1-CreERT2 mice were previously generated and crossed to $APC^{flox/flox}$, *Rosa26-mTomato/mGFP* (*R26-TGFP*), and *Rosa26-tdTomato* strains as previously described.[19] Tamoxifen was administered by oral gavage (3 doses of 6 mg every other day) to induce Cre recombinase activity in *Dclk1*-expressing cells. K19Cre(BAC) transgenic mice were previously generated[2] and crossed to $COX\text{-}1^{flox/flox}$ mice[72] (JAX#030884). Mice were housed in 12-hour-light/12-hour-dark cycles with controlled temperature (19 °C–22 °C) and humidity (40%–60%). All animal procedures were performed in accordance with the Animal Care and Use Committee at The University of Western Ontario.

DSS Colitis Model and Drug Treatments

To induce experimental colitis, 8-week-old mice were treated with 2.5% (wt/vol) DSS (molecular weight, 36,000–50,000, Gojira) in the drinking water for 5 days. Mice were treated with NSAIDs 3 times during DSS and every day post-DSS until experimental endpoints. Mice were sacrificed 12 to 14 weeks post-DSS for tumor experiments,

Figure 7. (*See previous page*). Low-dose aspirin does not exacerbate DSS colitis. (*A*) Schematic illustration of the DSS colitis model with low-dose aspirin treatment. C57Bl/6 mice were treated with aspirin during and post-DSS and analyzed on day 8. (*B*) Representative images of hematoxylin and eosin staining (*top*) and Ki67+ cell staining (*bottom*) for mice treated with DSS and/or aspirin at day 8. (*C*) Quantification for the percentage of damaged histological area in mice treated with DSS and/or aspirin. Data are presented as mean ± SEM, and dots represent biologically independent animals (control, n = 5; aspirin, n = 5; DSS, n = 5; DSS + aspirin, n = 6). (*D*) Quantification for the number of Ki67+ cells per colonic crypt (*right*) in mice treated with DSS and/or aspirin. Data are presented as mean ± SEM, and dots represent biologically independent animals (control, n = 6; aspirin, n = 7; DSS, n = 8; DSS + aspirin, n = 4). (*E*) Measurement of MPO activity in colonic tissue of mice treated with DSS and/or aspirin. Data are presented as mean ± SEM, and dots represent biologically independent animals (control, n = 12; aspirin, n = 11; DSS, n = 15; DSS + aspirin, n = 15). (*F*) Heatmap showing the relative protein levels of inflammatory cytokines and chemokines in colonic tissue of mice treated with DSS or DSS plus aspirin compared with control. Data are presented as mean ± SEM, and dots represent biologically independent animals (control, n = 5; DSS, n = 3; DSS + aspirin, n = 6). (*G*) Quantification of the number of inflammatory cytokines or chemokines presented in (*F*), which are significantly upregulated in mice treated with DSS relative to DSS + aspirin (4), those which are significantly upregulated in DSS + aspirin relative to DSS (2), or those which are non-significantly changed (26). (*H*) Heatmap showing the relative mRNA levels of inflammatory cytokines in colonic tissue of mice treated with DSS or DSS plus aspirin compared with control. (*I*) Schematic illustration of the DSS colitis model with low-dose aspirin treatment. C57Bl/6 mice were treated with aspirin during and post-DSS and analyzed on day 19. (*J*) Representative images of hematoxylin and eosin staining of colonic tissue of mice treated with DSS and/or aspirin at day 19. (*K*) Quantification for the percentage of damaged histological area in mice treated with DSS and/or aspirin. Data are presented as mean ± SEM, and dots represent biologically independent animals (control, n = 5; aspirin, n = 5; DSS, n = 5; DSS + aspirin, n = 5). (*L*) Measurement of MPO activity in colonic tissue of mice treated with DSS and/or aspirin. Data are presented as mean ± SEM, and dots represent biologically independent animals (control, n = 6; aspirin, n = 5; DSS, n = 5; DSS + aspirin, n = 5). (*M*) Changes in body weight expressed as percentage of initial weight of mice treated with DSS and/or aspirin (control, n = 6; aspirin, n = 5; DSS, n = 5; DSS + aspirin, n = 5). Data are presented as mean ± SEM.

and 1 or 3 days post-DSS for acute experiments. NSAIDs used were: aspirin (25 mg/kg; Sigma), celecoxib (6 mg/kg, 50 mg/kg; Sigma), rofecoxib (5 mg/kg, 15 mg/kg; ApexBio), SC-560 (10 mg/kg; Abcam), indomethacin (1 mg/kg; Abcam), and respective vehicles. The drug doses were selected based on those that were previously reported to be equivalent to low- and high-dose NSAIDs in patients based on plasma concentrations, calculated human equivalent doses, and/or equipotent COX inhibition.[73–78] For lineage tracing studies, mice were treated with Misoprostol (15 μg i.p., Cayman Chemicals) or SC79 (20 mg/kg i.p., Cayman Chemicals) daily for 5 consecutive days.

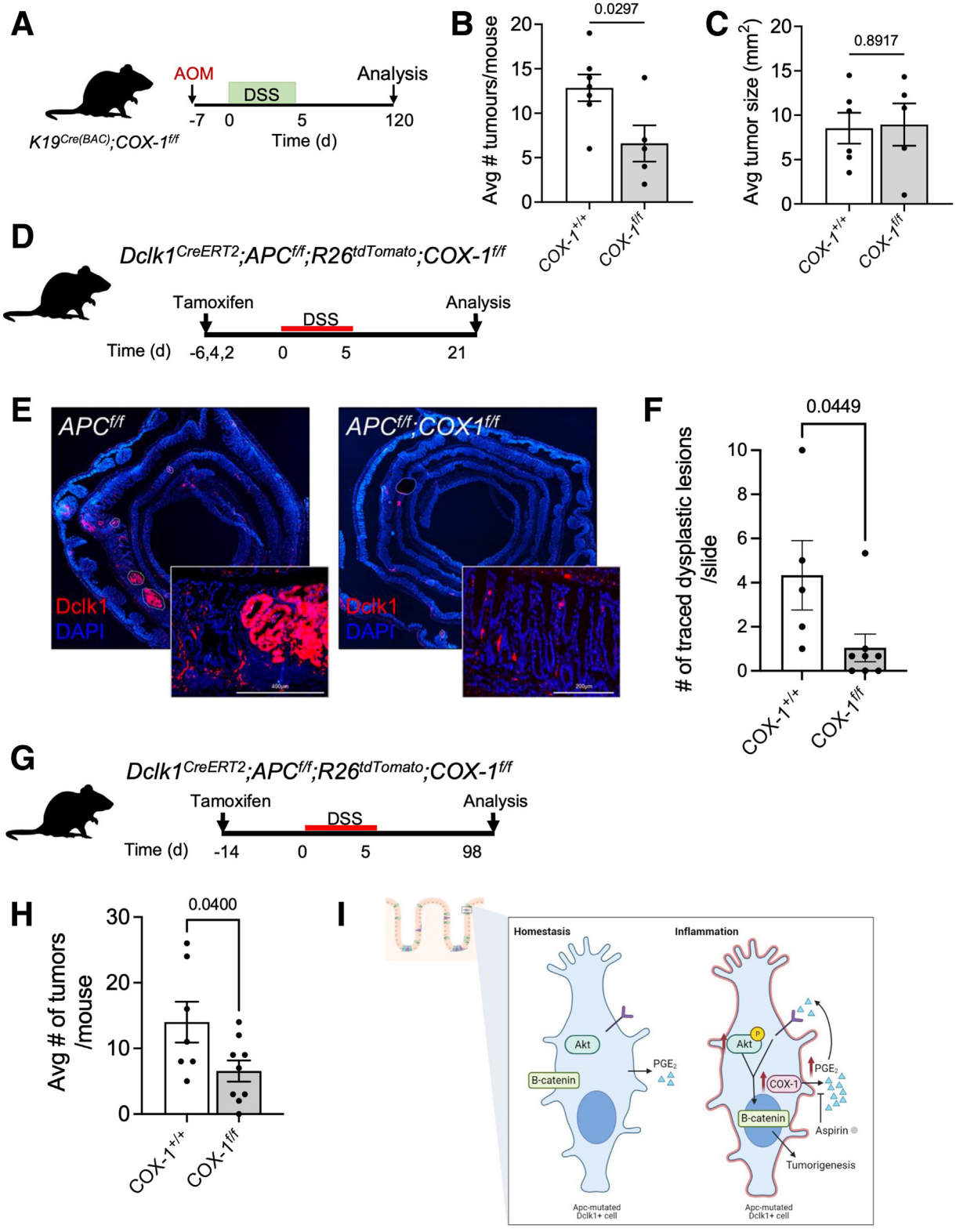

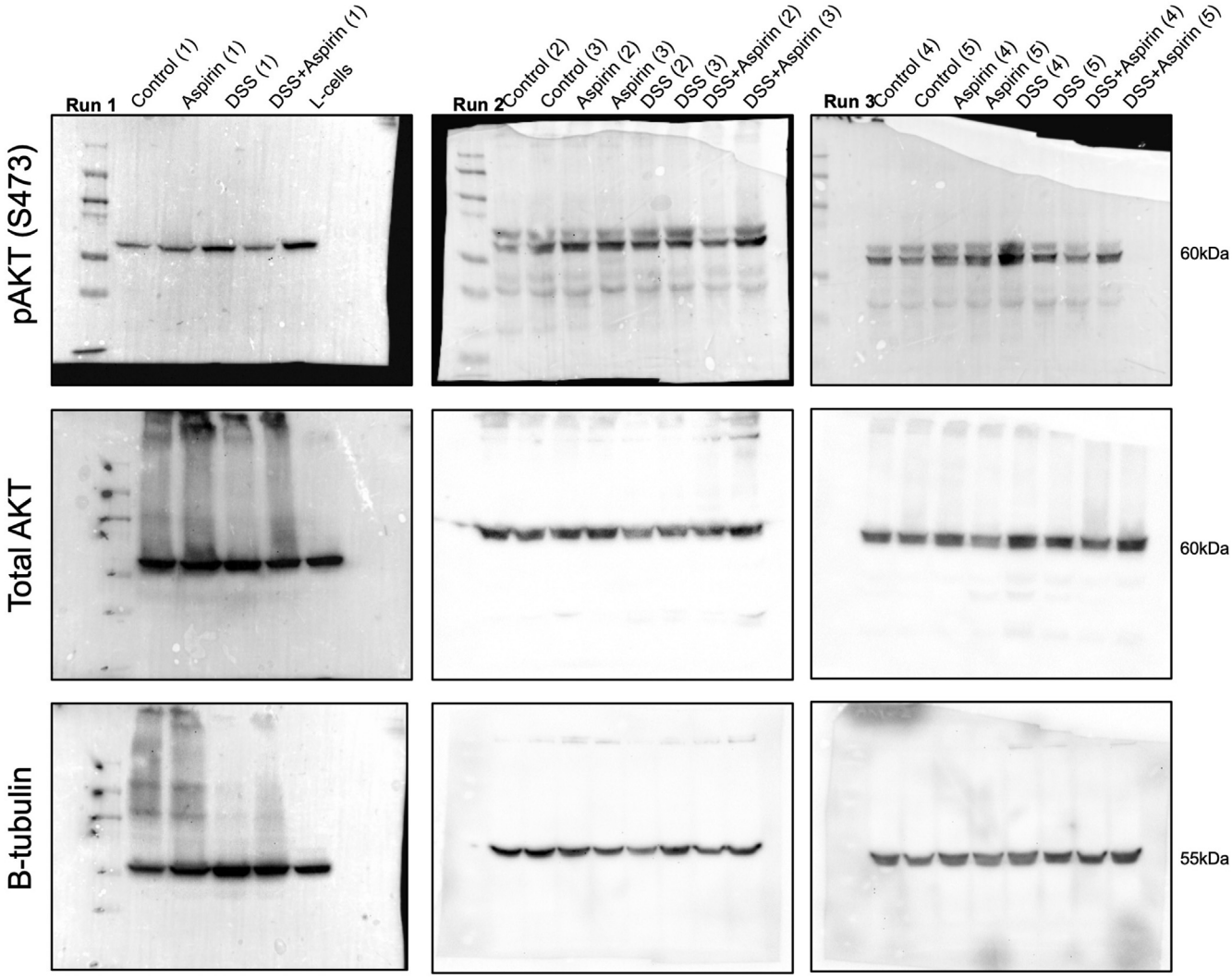

Figure 9. Western blots. (*A*) Raw data for Western blots using phospho-Akt (S473), total Akt, and B-tubulin anti-bodies.

MPO Assay

Colonic MPO activity was measured as previously described.[79,80] Briefly, fresh colonic tissue was harvested and weighed. Samples were homogenized in hexadecyltrimethylammonium bromide (HTAB) buffer (0.5% HTAB in 50 mM potassium phosphate buffer, pH 6.0) and centrifuged at 13,400 rpm for 6 minutes at 4 °C. Supernatant was collected and loaded in triplicate to a 96-well plate. *O*-dianisidine dihydrochloride solution (0.167 mg/mL *o*-dianisidine in 50 mM potassium phosphate buffer, pH 6.0) containing 0.0005% hydrogen peroxide was added to each well. Absorbance was measured at 450 nm using the Perkin Elmer Wallac 1420 Victor2 Microplate Reader (GMI). MPO activity was calculated as units of MPO activity/mg tissue, where 1 unit of MPO activity is equal to 1 μmol of peroxidase degraded per minute at 25 °C.

Figure 8. (***See previous page***). **Loss of COX-1 inhibits inflammation-associated cancer.** (*A*) Schematic illustration for the treatment of *K19$^{Cre(BAC)}$;COX-1$^{f/f}$* mice with AOM/DSS. (*B–C*) Colonic tumor number (*left*) and size (*right*) of *K19$^{Cre(BAC)}$;COX-1$^{f/f}$* mice relative to Cre-negative (*COX-1$^{+/+}$*) littermates. Data are presented as mean ± SEM, and dots represent biologically independent animals (*COX-1$^{+/+}$*, n = 3; *COX-1$^{f/f}$*, n = 5). (*D*) Schematic illustration for the treatment of *Dclk1^{CreERT2};APC$^{f/f}$;COX-1$^{f/f}$* mice with 1.5% DSS. (*E*) Representative images of colonic sections of *Dclk1^{CreERT2};APC$^{f/f}$* mice with or without COX-1 KO showing a dysplastic lesion in COX-1-WT mice and single Dclk1+ cells in *COX-1$^{f/f}$* mice. (*F*) Average number of dysplastic lesions per slide between *Dclk1^{CreERT2};APC$^{f/f}$* mice with or without COX-1 KO (COX-1$^{+/+}$, n = 5; COX-1$^{f/f}$, n = 8). (*G*) Schematic illustration for the treatment of *Dclk1^{CreERT2};APC$^{f/f}$;COX-1$^{f/f}$* mice with 2.5% DSS for tumor induction. (*H*) Average colonic tumor number between *Dclk1^{CreERT2};APC$^{f/f}$* mice with or without COX-1 KO (COX1$^{+/+}$, n = 7; COX-1$^{f/f}$, n = 9). (*I*) Working model for our proposed model of Dclk1+ cell-derived inflammation-associated tumorigenesis. Figure generated with Biorender.com.

Table 1. Real-Time Polymerase Chain Reaction Primers

Gene	Forward	Reverse
Gapdh	GACATCAAGAAGGTGGTGAAGCAG	ATACCAGGAAATGAGCTTGACAAA
Cox-1	CACAACACTTCACCCACCAG	AGAGCCGCAGGTGATACTGT
Cox-2	GCTGCCCGACACCTTCAACATT	CACATTTCTTCCCCCAGCAACC
Lgr5	GACGCTGGGTTATTTCAAGTTCAA	CAGCCAGCTACCAAATAGGTGCTC
Dclk1	AGCACTGCAGCAGGAGTTTCTG	AGTCCTCCGATTCCGAGTTCAA
C-myc	CCCACCACCAGCAGCGACTC	CAGTGGGCTGTGCGGAGGTT
Cyclin D1	GCAGAAGGAGATTGTGCCATCC	AGGAAGCGGTCCAGGTAGTTCA
PPAR-d	ATGGAACAGCCACAGGAGGA	ATCACAGCCCATCTGCAGCT

Quantitative Reverse Transcription Polymerase Chain Reaction

Total RNA was extracted from colonic tissue using TRIzol reagent (Invitrogen). RNA from DSS-treated mice was purified with lithium chloride as previously described, with some modifications.[81] Briefly, RNA was incubated with 8 M LiCl for 45 minutes at −20 °C, centrifuged at 15,000 rpm for 15 minutes, washed with 75% ethanol, and resuspended in nuclease-free water. RNA concentration was determined using the NanoDrop One Microvolume UV-Vis Spectrophotometer (Thermo Fisher Scientific). cDNA was synthesized using 1 μg RNA and was performed using iScript cDNA Synthesis Kit (Bio-Rad). Reverse transcription polymerase chain reaction (RT-PCR) was carried out in triplicate using PowerUp SYBR Green Master Mix (Thermo Fisher) and ViiA QuantStudio 5 (Thermo Fisher). See Table 1 for complete list of primers used.

Histology, Immunohistochemistry, and Immunofluorescence

Tissues were collected, fixed in formalin, embedded in paraffin, and sectioned at 5-μm thick onto glass slides. Tissue sections were deparaffinized in xylene and rehydrated in decreasing concentrations of ethanol. For histology, tissues were stained with CAT hematoxylin (Biocare Medical) and Eosin Y (Sigma) and were subsequently rehydrated and mounted using Permount (Fisher Scientific) for imaging. Percent damaged area was calculated based on the sum of areas with epithelial damage over total tissue area for each section. For analysis of endogenous fluorescence, harvested colonic tissue was fixed in 4% paraformadehyde for 4 to 6 hours and cryoprotected in 30% sucrose/phosphate buffered saline (PBS) for 24 hours. Tissues were embedded in OCT (4583, Sakura), frozen, and sectioned at 5 μm using the Leica CM3050 cryostat (Leica Biosystems). Frozen sections were rehydrated in PBS for 5 minutes at room temperature and mounted using Vectashield Mounting Medium containing DAPI (Vector Laboratories). For immunohistochemistry (IHC) and immunofluorescence, antigen retrieval was performed by boiling slides the microwave in Tris-EDTA buffer (pH 9.0) for formalin-fixed paraffin-embedded (FFPE) sections and in sodium citrate buffer (pH 6.0) for frozen sections. For IHC, slides were incubated in 3% hydrogen peroxide in methanol to quench endogenous peroxidase activity. Slides were rinsed with PBS and blocked with 5% normal horse serum. Primary antibodies were diluted in blocking solution and slides were incubated overnight at 4 °C. Using R.T.U. Vectastain Universal Elite ABC Kit (Vector Laboratories), biotinylated secondary antibody was applied for 1 hour at room temperature, followed by ABC reagent for 30 minutes. ImmPACT DAB Substrate (Vector Laboratories) was used as the peroxidase substrate solution. Slides were counterstained with CAT hematoxylin, rehydrated, and mounted using Permount. For immunofluorescence, slides were permeabilized in 0.2% Triton-X in PBS and blocked using 10% normal goat serum for 30 minutes at room temperature. Primary antibodies were diluted in blocking solution and incubated overnight at 4 °C. Secondary antibodies were diluted in blocking solution and incubated for 1 hour at room temperature. Slides were counterstained and mounted using Vectashield Mounting Medium containing DAPI (Vector Laboratories). See Table 2 for complete list of antibodies used.

Table 2. Antibodies

Name	Type	Concentration	Vendor	CAT No.
Anti-DCAMKL1	Rabbit polyclonal	1:200	Abcam	ab31704
Anti-Ki67	Rabbit monoclonal	1:200	Abcam	ab16667
Anti-RFP	Rabbit polyclonal	1:200	Rockland Inc	Ab124754
Alexa Fluor 488 (Goat anti-rabbit)	Goat polyclonal	1:200	Thermo Fisher	AB143165
Anti-phospho-Akt (Ser473)	Rabbit polyclonal	1:1000	Cell Signaling Technology	9271S
Anti-Akt	Rabbit polyclonal	1:1000	Cell Signaling Technology	9272S
Anti-Beta-Tubulin	Rabbit polyclonal	1:1000	Cell Signaling Technology	2146S

Intestinal Organoid Culture System

Small intestinal crypt cultures were performed as previously described.[82] Briefly, the small intestine was harvested, villi were scraped off, and tissue was washed 5 times with cold PBS. Tissues were incubated for 1 hour in 2.5 mM EDTA in PBS, followed by mechanical agitation of intestinal fragments in 10% fetal bovine serum (FBS)/PBS. Supernatant containing crypts was subsequently passed through a 70-μM filter (Fisher). Crypt fractions were centrifuged at 800 rpm for 5 minutes, resuspended in conditioned media, and finally centrifuged at 600 rpm for 5 minutes. Crypts were embedded in Matrigel and plated on pre-warmed 48-well plates. After polymerization, 250 uL of Dulbecco's Modified Eagle's Medium/F12 containing N2 supplement (1×; Thermo Fisher), B27 supplement (1×; Thermo Fisher), *N*-acetylcysteine (1 μM; Sigma), Glutamax (1×; Thermo Fisher), HEPES (10 μM; Gibco), and penicillin/streptomycin (500 μg/mL, Life Technologies) was added to plated crypts and refreshed every 4 days. Media was supplemented with EGF 50 ng/mL (Invitrogen), mNoggin 100 ng/mL (Peprotech), and R-Spondin 1 ug/mL every 2 days. For lineage tracing experiments, organoids were treated with 4-hydroxytamoxifen (dose) for 48 hours, washed, and treated with PGE_2 (10 μM; Abcam), SC79 (Cayman Chemicals; 8 μg/mL), and/or MK-2206 (3 μM) in fresh media. For epithelial injury experiments, organoids were treated with doxorubicin (dose) dissolved in the media for 3 hours. Organoids were then washed 3 times with PBS before being treated with PGE_2 (10 μM; Abcam), SC79 (Cayman Chemicals; 8 μg/mL) or both, dissolved in normal media.

AOM DSS Model of Tumorigenesis

As previously described,[83] 6-week-old C57Bl/6J mice were treated with azoxymethane (10 mg/kg, i.p.) on day 0, followed by 5 days of 2.5% DSS in the drinking water starting on day 7. Colonic and tumor tissues were harvested at week 20 for analysis.

Multiplex Cytokine Array

Total protein concentration of homogenized colonic tissue was determined using the DC Protein Assay (Bio-Rad). Levels of eotaxin, G-CSF, GM-CSF, IFNgamma, IL-1alpha, IL-1beta, IL-2, IL-3, IL-4, IL-5, IL-6, IL-7, IL-9, IL-10, IL-12 (p40), IL-12 (p70), IL-13, IL-15, IL-17A, IL-17E, IL-17F, IL-21, IL-22, IL-23, IL-27, IL-28B, IL-31, IL-33, IP-10, KC, LIF, LIX, MCP-1, M-CSF, MIG, MIP-1alpha, MIP-1beta, MIP-2, MIP-3a, RANTES, TNF-alpha, and VEGF were determined using a Multiplexing LASER Bead Assay (Eve Technologies Corporation).

Multiple Reaction Monitoring LC-MS Pro-inflammatory Lipid Signaling Panel

Levels of eicosanoids were measured in colonic tissue using multiple reaction monitoring (MRM) coupled with LC-MS as previously described.[84]

Western Blot

Western blots were performed as previously described[85] with some modifications. Briefly, 25 to 30 mg of colonic tissue was collected and homogenized in 200uL standard RIPA buffer with 0.5 mM NaF and 0.1 mM Na_3VO_4 for protein isolation. Protein was quantified using a Bradford assay (BioRad). Twenty μg protein lysates were loaded on 8% SDS-PAGE gel and transferred to nitrocellulose membrane (BioRad) using a wet electroblotting system (BioRad). The membrane was incubated using the manufacturer protocols for p-Akt (S473) (CAT# 9271S), Akt (CAT# 9272S), and Beta-tubulin (CAT#2146S) antibodies (Cell Signaling Technologies). The membrane was rinsed briefly in enhanced chemiluminescence substrate (BioRad) and imaged using the BioRad ChemiDoc MP Image System. Raw data for Western blots can be found in Figure 9.

Imaging

Imaging was performed using the EVOS FL Auto Imaging System (Thermo Fisher) or Nikon Confocal Microscope. To conform with colorblindness, all images from mTmG reporter mice were changed so DAPI is blue, RFP is magenta, and GFP is green.

The GEO Data Sets

Publicly available gene expression data used in this study were accessed from the NCBI GEO under the accessing codes: GSE37283, GSE75214, GSE31106, and GSE44904. For GSE37283, the data analyzed for this study included RNA expression profiling by microarray of colonic biopsies from 5 healthy controls, 4 patients with quiescent UC, and 11 patients with UC that harbored a remote neoplastic lesion.

For GSE75214, the data analyzed for this study included RNA expression profiling by microarray of colonic mucosal biopsies from 11 healthy controls, 97 patients with active UC, and 23 patients with inactive UC. Disease activity was based on endoscopic findings with active disease defined as a Mayo score of 2 or greater.

For GSE31106, colonic samples (inflamed, dysplastic, and tumors) were collected at 6 different timepoints (weeks 0, 2, 4, 6, 8, and 20) to determine the expression pattern with the progression from colitis to colitis-associated dysplasia to colitis-associated tumors.

For GSE44904, colonic samples were collected from an untreated control group or colonic tumors from AOM/DSS-treated mice, both on day 100 post treatment initiation.

Statistics

Statistical analysis was performed using an unpaired Student *t*-test when comparing 2 groups and using a 1-way analysis of variance (ANOVA) when comparing 3 or more groups. Analyses were done using GraphPad Prism software version 9.0 (GraphPad Software Inc). A *P*-value of less than .05 was considered statistically significant.

References

1. Barker N, van Es JH, Kuipers J, et al. Identification of stem cells in small intestine and colon by marker gene Lgr5. Nature 2007;449:1003–1007.
2. Asfaha S, Hayakawa Y, Muley A, et al. Krt19(+)/Lgr5(-) cells are radioresistant cancer-initiating stem cells in the colon and intestine. Cell Stem Cell 2015; 16:627–638.
3. Ayyaz A, Kumar S, Sangiorgi B, et al. Single-cell transcriptomes of the regenerating intestine reveal a revival stem cell. Nature 2019;569:121–125.
4. Castillo-Azofeifa D, Fazio EN, Nattiv R, et al. Atoh1(+) secretory progenitors possess renewal capacity independent of Lgr5(+) cells during colonic regeneration. EMBO J 2019;38:e99984.
5. Yui S, Azzolin L, Maimets M, et al. YAP/TAZ-dependent reprogramming of colonic epithelium links ECM remodeling to tissue regeneration. Cell Stem Cell 2018; 22:35–49.e7.
6. Murata K, Jadhav U, Madha S, et al. Ascl2-dependent cell dedifferentiation drives regeneration of ablated intestinal stem cells. Cell Stem Cell 2020;26(3):377–390.e6.
7. Deng F, Peng L, Li Z, et al. YAP triggers the Wnt/beta-catenin signalling pathway and promotes enterocyte self-renewal, regeneration and tumorigenesis after DSS-induced injury. Cell Death Dis 2018;9:153.
8. Gregorieff A, Liu Y, Inanlou MR, et al. Yap-dependent reprogramming of Lgr5(+) stem cells drives intestinal regeneration and cancer. Nature 2015;526:715–718.
9. Nusse YM, Savage AK, Marangoni P, et al. Parasitic helminths induce fetal-like reversion in the intestinal stem cell niche. Nature 2018;559:109–113.
10. Sato T, Sase M, Ishikawa S, et al. Characterization of radioresistant epithelial stem cell heterogeneity in the damaged mouse intestine. Sci Rep 2020;10:8308.
11. Wells JM, Watt FM. Diverse mechanisms for endogenous regeneration and repair in mammalian organs. Nature 2018;557:322–328.
12. Clevers H, Loh KM, Nusse R. Stem cell signaling. An integral program for tissue renewal and regeneration: Wnt signaling and stem cell control. Science 2014;346:1248012.
13. Cordero JB, Sansom OJ. Wnt signalling and its role in stem cell-driven intestinal regeneration and hyperplasia. Acta Physiol (Oxf) 2012;204:137–143.
14. Perochon J, Carroll LR, Cordero JB. Wnt signalling in intestinal stem cells: lessons from mice and flies. Genes (Basel) 2018;9:138.
15. Harnack C, Berger H, Antanaviciute A, et al. R-spondin 3 promotes stem cell recovery and epithelial regeneration in the colon. Nat Commun 2019;10:4368.
16. Suh HN, Kim MJ, Jung YS, et al. Quiescence exit of Tert(+) stem cells by Wnt/beta-catenin is indispensable for intestinal regeneration. Cell Rep 2017;21(9):2571–2584.
17. Valentin-Vega YA, Okano H, Lozano G. The intestinal epithelium compensates for p53-mediated cell death and guarantees organismal survival. Cell Death Differ 2008;15:1772–1781.
18. Barker N, Ridgway RA, van Es JH, et al. Crypt stem cells as the cells-of-origin of intestinal cancer. Nature 2009; 457:608–611.
19. Westphalen CB, Asfaha S, Hayakawa Y, et al. Long-lived intestinal tuft cells serve as colon cancer-initiating cells. J Clin Invest 2014;124:1283–1295.
20. Schwitalla S, Fingerle AA, Cammareri P, et al. Intestinal tumorigenesis initiated by dedifferentiation and acquisition of stem-cell-like properties. Cell 2013;152:25–38.
21. Davis H, Irshad S, Bansal M, et al. Aberrant epithelial GREM1 expression initiates colonic tumorigenesis from cells outside the stem cell niche. Nat Med 2015;21:62–70.
22. Verhagen MP, Joosten R, Schmitt M, et al. Non-stem cell lineages as an alternative origin of intestinal tumorigenesis in the context of inflammation. Nat Genet 2024; 56:1456–1467.
23. Eaden JA, Abrams KR, Mayberry JF. The risk of colorectal cancer in ulcerative colitis: a meta-analysis. Gut 2001;48:526–535.
24. Ekbom A, Helmick C, Zack M, Adami HO. Ulcerative colitis and colorectal cancer. A population-based study. N Engl J Med 1990;323:1228–1233.
25. Kraus S, Arber N. Inflammation and colorectal cancer. Curr Opin Pharmacol 2009;9:405–410.
26. Shanahan F. Relation between colitis and colon cancer. Lancet 2001;357:246–247.
27. Fujita M, Matsubara N, Matsuda I, et al. Genomic landscape of colitis-associated cancer indicates the impact of chronic inflammation and its stratification by mutations in the Wnt signaling. Oncotarget 2018;9:969–981.
28. Han J, Soletti RC, Sadarangani A, et al. Nuclear expression of beta-catenin promotes RB stability and resistance to TNF-induced apoptosis in colon cancer cells. Mol Cancer Res 2013;11:207–218.
29. Kameyama H, Nagahashi M, Shimada Y, et al. Genomic characterization of colitis-associated colorectal cancer. World J Surg Oncol 2018;16:121.
30. Tanaka T, Kohno H, Suzuki R, et al. A novel inflammation-related mouse colon carcinogenesis model induced by azoxymethane and dextran sodium sulfate. Cancer Sci 2003;94:965–973.
31. Gao Y, Li X, Yang M, et al. Colitis-accelerated colorectal cancer and metabolic dysregulation in a mouse model. Carcinogenesis 2013;34:1861–1869.
32. Pekow J, Dougherty U, Huang Y, et al. Gene signature distinguishes patients with chronic ulcerative colitis harboring remote neoplastic lesions. Inflamm Bowel Dis 2013;19:461–470.
33. Castellone MD, Teramoto H, Williams BO, et al. Prostaglandin E2 promotes colon cancer cell growth through a Gs-axin-beta-catenin signaling axis. Science 2005; 310:1504–1510.
34. Goessling W, North TE, Loewer S, et al. Genetic interaction of PGE2 and Wnt signaling regulates developmental specification of stem cells and regeneration. Cell 2009;136:1136–1147.
35. Peng X, Li J, Tan S, et al. COX-1/PGE(2)/EP4 alleviates mucosal injury by upregulating beta-arr1-mediated Akt signaling in colitis. Sci Rep 2017;7:1055.
36. Wang D, Wang H, Shi Q, et al. Prostaglandin E(2) promotes colorectal adenoma growth via transactivation of the nuclear peroxisome proliferator-activated receptor delta. Cancer Cell 2004;6:285–295.

37. Vancamelbeke M, Vanuytsel T, Farre R, et al. Genetic and transcriptomic bases of intestinal epithelial barrier dysfunction in inflammatory bowel disease. Inflamm Bowel Dis 2017;23:1718–1729.
38. Jo H, Mondal S, Tan D, et al. Small molecule-induced cytosolic activation of protein kinase Akt rescues ischemia-elicited neuronal death. Proc Natl Acad Sci U S A 2012;109:10581–10586.
39. Sheahan BJ, Freeman AN, Keeley TM, et al. Epithelial Regeneration After Doxorubicin Arises Primarily From Early Progeny of Active Intestinal Stem Cells. Cell Mol Gastroenterol and Hepatol 2021;12:119–140.
40. Buczacki SJ, Zecchini HI, Nicholson AM, et al. Intestinal label-retaining cells are secretory precursors expressing Lgr5. Nature 2013;495:65–69.
41. van Es JH, Sato T, van de Wetering M, et al. Dll1+ secretory progenitor cells revert to stem cells upon crypt damage. Nat Cell Biol 2012;14:1099–1104.
42. Tetteh PW, Kretzschmar K, Begthel H, et al. Generation of an inducible colon-specific Cre enzyme mouse line for colon cancer research. Proc Natl Acad Sci U S A 2016; 113:11859–11864.
43. Tetteh PW, Basak O, Farin HF, et al. Replacement of lost Lgr5-positive stem cells through plasticity of their enterocyte-lineage daughters. Cell Stem Cell 2016; 18:203–213.
44. Schmitt M, Schewe M, Sacchetti A, et al. Paneth cells respond to inflammation and contribute to tissue regeneration by acquiring stem-like features through SCF/c-Kit signaling. Cell Rep 2018;24:2312–2328.e7.
45. Schonhoff SE, Giel-Moloney M, Leiter AB. Neurogenin 3-expressing progenitor cells in the gastrointestinal tract differentiate into both endocrine and non-endocrine cell types. Dev Biol 2004;270:443–454.
46. Yan KS, Janda CY, Chang J, et al. Non-equivalence of Wnt and R-spondin ligands during Lgr5(+) intestinal stem-cell self-renewal. Nature 2017;545:238–242.
47. Kim HB, Kim M, Park YS, et al. Prostaglandin E(2) activates YAP and a positive-signaling loop to promote colon regeneration after colitis but also carcinogenesis in mice. Gastroenterology 2017;152:616–630.
48. Frisch BJ, Porter RL, Gigliotti BJ, et al. In vivo prostaglandin E2 treatment alters the bone marrow microenvironment and preferentially expands short-term hematopoietic stem cells. Blood 2009;114:4054–4063.
49. Gupta RA, Dubois RN. Colorectal cancer prevention and treatment by inhibition of cyclooxygenase-2. Nat Rev Cancer 2001;1:11–21.
50. Gupta R, Bhatt LK, Johnston TP, Prabhavalkar KS. Colon cancer stem cells: potential target for the treatment of colorectal cancer. Cancer Biol Ther 2019; 20:1068–1082.
51. Hoggatt J, Singh P, Sampath J, Pelus LM. Prostaglandin E2 enhances hematopoietic stem cell homing, survival, and proliferation. Blood 2009;113:5444–5455.
52. Kuroda H, Mabuchi S, Yokoi E, et al. Prostaglandin E2 produced by myeloid-derived suppressive cells induces cancer stem cells in uterine cervical cancer. Oncotarget 2018;9:36317–36330.
53. Lee BC, Kim HS, Shin TH, et al. PGE2 maintains self-renewal of human adult stem cells via EP2-mediated autocrine signaling and its production is regulated by cell-to-cell contact. Sci Rep 2016;6:26298.
54. Fan Y, Davidson LA, Callaway ES, et al. Differential effects of 2- and 3-series E-prostaglandins on in vitro expansion og Lgr5+ colonic stem cells. Carcinogenesis 2014;35:606–612.
55. Buchanan FG, Wang D, Bargiacchi F, DuBois RN. Prostaglandin E2 regulates cell migration via the intracellular activation of the epidermal growth factor receptor. J Biol Chem 2003;278:35451–35457.
56. Torrance CJ, Jackson PE, Montgomery E, et al. Combinatorial chemoprevention of intestinal neoplasia. Nat Med 2000;6:1024–1028.
57. Hayakawa Y, Tsuboi M, Asfaha S, et al. BHLHA15-positive secretory precursor cells can give rise to tumors in intestine and colon in mice. Gastroenterology 2019;156:1066–1081.e16.
58. Oshima M, Dinchuk JE, Kargman SL, et al. Suppression of intestinal polyposis in Apc delta716 knockout mice by inhibition of cyclooxygenase 2 (COX-2). Cell 1996; 87:803–809.
59. Phillips RK, Wallace MH, Lynch PM, et al, FAP Study Group. A randomised, double blind, placebo controlled study of celecoxib, a selective cyclooxygenase 2 inhibitor, on duodenal polyposis in familial adenomatous polyposis. Gut 2002;50:857–860.
60. Roulis M, Kaklamanos A, Schernthanner M, et al. Paracrine orchestration of intestinal tumorigenesis by a mesenchymal niche. Nature 2020;580:524–529.
61. He X, Smith SE, Chen S, et al. Tumor-initiating stem cell shapes its microenvironment into an immunosuppressive barrier and pro-tumorigenic niche. Cell Rep 2021;36: 109674.
62. Biancone L, Tosti C, De Nigris F, et al. Selective cyclooxygenase-2 inhibitors and relapse of inflammatory bowel disease. Gastroenterology 2003;125:637–638.
63. Hegazi RA, Mady HH, Melhem MF, et al. Celecoxib and rofecoxib potentiate chronic colitis and premalignant changes in interleukin 10 knockout mice. Inflamm Bowel Dis 2003;9:230–236.
64. Ishikawa TO, Oshima M, Herschman HR. Cox-2 deletion in myeloid and endothelial cells, but not in epithelial cells, exacerbates murine colitis. Carcinogenesis 2011; 32:417–426.
65. Matuk R, Crawford J, Abreu MT, et al. The spectrum of gastrointestinal toxicity and effect on disease activity of selective cyclooxygenase-2 inhibitors in patients with inflammatory bowel disease. Inflamm Bowel Dis 2004; 10:352–356.
66. Zhang L, Lv Y, Ye S, Dong X. [Mechanism of exacerbation of colonic damage in experimental colitis treated with celecoxib]. Beijing Da Xue Xue Bao Yi Xue Ban 2008;40:195–199.
67. Sakamoto C. Roles of COX-1 and COX-2 in gastrointestinal pathophysiology. J Gastroenterol 1998; 33:618–624.
68. Wallace JL, Bak A, McKnight W, et al. Cyclooxygenase 1 contributes to inflammatory responses in rats and mice:

implications for gastrointestinal toxicity. Gastroenterology 1998;115:101–109.
69. McAdam BF, Mardini IA, Habib A, et al. Effect of regulated expression of human cyclooxygenase isoforms on eicosanoid and isoeicosanoid production in inflammation. J Clin Invest 2000;105:1473–1482.
70. Chulada PC, Thompson MB, Mahler JF, et al. Genetic disruption of Ptgs-1, as well as Ptgs-2, reduces intestinal tumorigenesis in Min mice. Cancer Res 2000; 60:4705–4708.
71. Cohn SM, Schloemann S, Tessner T, et al. Crypt stem cell survival in the mouse intestinal epithelium is regulated by prostaglandins synthesized through cyclooxygenase-1. J Clin Invest 1997;99:1367–1379.
72. Crescente M, Armstrong PC, Kirkby NS, et al. Profiling the eicosanoid network that underlie the anti- and prothrombotic effects of aspirin. The FASEB journal 2020; 34:10027–10040.
73. El-Medany A, Mahgoub A, Mustafa A, et al. The effects of selective cyclooxygenase-2 inhibitors, celecoxib and rofecoxib, on experimental colitis induced by acetic acid in rats. Eur J Pharmacol 2005;507:291–299.
74. Laudanno OM, Cesolari JA, Esnarriaga J, et al. Gastrointestinal damage induced by celecoxib and rofecoxib in rats. Dig Dis Sci 2001;46:779–784.
75. Nair AB, Jacob S. A simple practice guide for dose conversion between animals and human. J Basic Clin Pharm 2016;7:27–31.
76. Oshima M, Murai N, Kargman S, et al. Chemoprevention of intestinal polyposis in the Apcdelta716 mouse by rofecoxib, a specific cyclooxygenase-2 inhibitor. Cancer Res 2001;61:1733–1740.
77. Rohwer N, Kuhl AA, Ostermann AI, et al. Effects of chronic low-dose aspirin treatment on tumor prevention in three mouse models of intestinal tumorigenesis. Cancer Med 2020;9:2535–2550.
78. Smith CJ, Zhang Y, Koboldt CM, et al. Pharmacological analysis of cyclooxygenase-1 in inflammation. Proc Natl Acad Sci U S A 1998;95:13313–13318.
79. Kim JJ, Shajib MS, Manocha MM, et al. Investigating intestinal inflammation in DSS-induced model of IBD. J Vis Exp 2012;(60):3678.
80. Krawisz JE, Sharon P, Stenson WF. Quantitative assay for acute intestinal inflammation based on myeloperoxidase activity. Assessment of inflammation in rat and hamster models. Gastroenterology 1984;87:1344–1350.
81. Viennois E, Chen F, Laroui H, et al. Dextran sodium sulfate inhibits the activities of both polymerase and reverse transcriptase: lithium chloride purification, a rapid and efficient technique to purify RNA. BMC Res Notes 2013;6:360.
82. Sato T, Vries RG, Snippert HJ, et al. Single Lgr5 stem cells build crypt-villus structures in vitro without a mesenchymal niche. Nature 2009;459:262–265.
83. Tanaka T, Kohno H, Suzuki R, et al. A novel inflammation-related mouse colon carcinogenesis model induced by azoxymethane and dextran sodium sulfate. Cancer Sci 2003;94:965–973.
84. Meriwether D, Sulaiman D, Volpe C, et al. Apolipoprotein A-I mimetics mitigate intestinal inflammation in COX2-dependent inflammatory bowel disease model. J Clin Invest 2019;129:3670–3685.
85. Tamming RJ, Dumeaux V, Jiang Y, et al. Atrx deletion in neurons lead to sexually dimorphic dysregulation of miR-137 and spatial learning and memory deficits. Cell Rep 2020;31:107838.

Received May 17, 2024. Accepted January 22, 2025.

Correspondence
Address correspondence to: Samuel Asfaha, Western University, 800 Commissioners Rd East, Rm A143, Victoria Research Laboratory, London, ON NGA 5W9 Canada. e-mail: sasfaha2@uwo.ca.

CRediT Authorship Contributions
Hayley Joan Good, PhD (Conceptualization: Equal; Data curation: Lead; Formal analysis: Lead; Investigation: Lead; Methodology: Equal; Writing – original draft: Lead)
Frederikke V. Larsen (Data curation: Supporting; Writing – review & editing: Supporting)
Alice Eunjung Shin, PhD (Conceptualization: Supporting; Investigation: Supporting)
Liyue Zhang, MSc (Investigation: Supporting)
Mathieu Derouet (Data curation: Supporting; Writing – review & editing: Supporting)
David Meriwether, PhD (Data curation: Supporting; Formal analysis: Supporting)
Daniel L Worthley, MBBS, MPH, PhD (Writing – review & editing: Supporting)
Srinivasa T. Reddy, PhD (Data curation: Supporting; Supervision: Supporting)
Timothy Cragin Wang, MD (Resources: Supporting; Writing – review & editing: Supporting)
Samuel Asfaha, MD, PhD (Conceptualization: Lead; Methodology: Lead; Resources: Lead; Supervision: Lead; Writing – original draft: Equal; Writing – review & editing: Lead)

Conflicts of interest
The authors disclose no conflicts.

Funding
This work was supported by operating grants from Canadian Institutes of Health Research (CIHR) and Cancer Research Society awarded to Samuel Asfaha, Canadian Institutes of Health Research Studentship to Hayley Joan Good, and by the National Institutes of Health (NIH) U01-DK103155 awarded to Timothy Wang and Chandan Guha.